Reevaluation of IEEE Standard 605's Calculation of Short Circuit Force on Rigid Busbar Structures

1024226

Reevaluation of IEEE Standard 605's Calculation of Short Circuit Force on Rigid Busbar Structures

1024226

Technical Update, December 2012

EPRI Project Manager

R. Adapa

DISCLAIMER OF WARRANTIES AND LIMITATION OF LIABILITIES

THIS DOCUMENT WAS PREPARED BY THE ORGANIZATION(S) NAMED BELOW AS AN ACCOUNT OF WORK SPONSORED OR COSPONSORED BY THE ELECTRIC POWER RESEARCH INSTITUTE, INC. (EPRI). NEITHER EPRI, ANY MEMBER OF EPRI, ANY COSPONSOR, THE ORGANIZATION(S) BELOW, NOR ANY PERSON ACTING ON BEHALF OF ANY OF THEM:

(A) MAKES ANY WARRANTY OR REPRESENTATION WHATSOEVER, EXPRESS OR IMPLIED, (I) WITH RESPECT TO THE USE OF ANY INFORMATION, APPARATUS, METHOD, PROCESS, OR SIMILAR ITEM DISCLOSED IN THIS DOCUMENT, INCLUDING MERCHANTABILITY AND FITNESS FOR A PARTICULAR PURPOSE, OR (II) THAT SUCH USE DOES NOT INFRINGE ON OR INTERFERE WITH PRIVATELY OWNED RIGHTS, INCLUDING ANY PARTY'S INTELLECTUAL PROPERTY, OR (III) THAT THIS DOCUMENT IS SUITABLE TO ANY PARTICULAR USER'S CIRCUMSTANCE; OR

(B) ASSUMES RESPONSIBILITY FOR ANY DAMAGES OR OTHER LIABILITY WHATSOEVER (INCLUDING ANY CONSEQUENTIAL DAMAGES, EVEN IF EPRI OR ANY EPRI REPRESENTATIVE HAS BEEN ADVISED OF THE POSSIBILITY OF SUCH DAMAGES) RESULTING FROM YOUR SELECTION OR USE OF THIS DOCUMENT OR ANY INFORMATION, APPARATUS, METHOD, PROCESS, OR SIMILAR ITEM DISCLOSED IN THIS DOCUMENT.

REFERENCE HEREIN TO ANY SPECIFIC COMMERCIAL PRODUCT, PROCESS, OR SERVICE BY ITS TRADE NAME, TRADEMARK, MANUFACTURER, OR OTHERWISE, DOES NOT NECESSARILY CONSTITUTE OR IMPLY ITS ENDORSEMENT, RECOMMENDATION, OR FAVORING BY EPRI.

THE FOLLOWING ORGANIZATION, UNDER CONTRACT TO EPRI, PREPARED THIS REPORT:

FSU-Center for Advanced Power Systems (CAPS)

This is an EPRI Technical Update report. A Technical Update report is intended as an informal report of continuing research, a meeting, or a topical study. It is not a final EPRI technical report.

NOTE

For further information about EPRI, call the EPRI Customer Assistance Center at 800.313.3774 or e-mail askepri@epri.com.

Electric Power Research Institute, EPRI, and TOGETHER…SHAPING THE FUTURE OF ELECTRICITY are registered service marks of the Electric Power Research Institute, Inc.

ACKNOWLEDGMENTS

ABSTRACT

The ever-increasing demand for utility substations to increase their power throughput raises new concerns about the ability of existing station bus work to withstand the short circuit (SC) forces produced by the correspondingly higher fault current levels. The guidelines of IEEE Std. 605 for predicting maximum SC forces and stresses on rigid bus conductors, insulators, and supports have long been relied upon when designing substation bus systems. However, these guidelines are overly conservative in that they are based on only a static analysis of bus fault response and do not include the dynamic SC response. This report assesses the applicability of IEEE Std. 605 SC force calculations to conditions of high fault current by comparing IEEE Std. 605 predictions of SC force and stress on a single span of rigid bus, with finite element analysis predictions and measured values. This report also takes an extensive look at several alternatives to the use of the static analysis guidelines of IEEE Std. 605, which include the effects of bus dynamic SC response. The report concludes that, of the five hand calculation methods considered in this study, the Attri and Edgar Dynamic Stress Model for Bus Supports predicts most accurately the SC forces on busbars and their support structure with respect to measurements from nine experimental setups in the open literature.

EXECUTIVE SUMMARY

With the introduction of distributed generation (DG) to the utility industry, the power throughput requirements of substations have risen dramatically. As a consequence, the fault current levels in substation bus work have also increased significantly. The potential now exists for substation short circuit (SC) current levels to be as high as 100 kA. Such high SC current levels are of concern to substation designers because the electromagnetic (EM) fields that they generate can interact in ways that produce potentially damaging mechanical forces on bus structural elements.

In order to account for the presence of these mechanical forces during substation design, the IEEE has issued standards IEEE 605-1998 and IEEE 605-2008 that provide simple formulas for predicting the maximum static mechanical force due to SC currents on each span of both rigid and flexible busbar systems. When specifying insulator cantilever force requirements under SC conditions, it is common industry practice to simply use the SC force equations of IEEE Std. 605 with an overload factor of 1 [5]. This approach is widely accepted as resulting in bus designs that are overly conservative for the levels of SC current that are anticipated. With the increasing cost of substation construction/retrofit, there is renewed interest in alternative SC force/stress calculation methods that are less conservative than IEEE Std. 605.

This report describes a study to assess the applicability of IEEE Std. 605 SC force calculations to conditions of high fault current. The report also identifies five alternative SC force calculation methods to the static analysis of IEEE Std. 605 alone that include consideration of bus dynamic response:

- The Simplified Method of IEC-865-1 [6]

- The Detailed Method of IEC-865-1 [6]

- Attri and Edgar's Dynamic Stress Model for Bus Supports (that is, Attri-Edgar Method) [4]

- The Edgar Model [7]

- Admunsen, Oster, and Malten's Dynamic Maximum Response Factor (DMF) Model [5]

A comparative performance assessment of the five dynamic response methods and IEEE Std. 605 is described in the report. This assessment involved automating each method in MATLAB[1] and running the method's program with parameters for nine SC force measurement setups described in the open literature. The results include predictions of bus natural frequency, insulator cantilever force, and insulator bending stress from each.

Based on these results, this study concludes that:

- The methodology of IEEE Std. 605 remains valid even at high fault current levels.

- Including the consideration of bus dynamic response in the prediction of SC force can yield force estimates that are considerably less conservative than the static force calculations of IEEE Std. 605.

---

[1] MATLAB is a registered trademark of Math Works.

- In the calculation of bus assembly natural frequency, the Attri-Edgar Method is the only method that includes the contribution from the elasticity of the insulators and the bus. As a result, when the spring constants for the insulators are known, the Attri-Edgar Method yields the most accurate prediction of bus natural frequency among the methods studied.

- In the prediction of conductor bending stress, the method of IEEE Std. 605-1998 provided the most accurate results. However, the calculation of Attri-Edgar over-predicted consistently and might be the preferable approach with a correction factor.

- In the prediction of SC insulator cantilever force without reclosure, the Attri-Edgar Method produced the closest values to the measured data.

- In the prediction of SC insulator cantilever force with reclosure, the Attri-Edgar Method produced the closest values to the measured data (that do not drastically underestimate the forces).

Based on these conclusions, this study recommends that:

- The calculation of bus assembly natural frequency be computed using the Attri-Edgar Method when the insulator spring constants are available. When the spring constants are not known, IEEE Std. 605-2008 should be used.

- The calculation of insulator cantilever forces (and also bus conductor bending stress if a proper correction factor can be found) should be computed with the Attri-Edgar Method. Because of this recommendation, the code for the Attri-Edgar Method written in MATLAB is provided in Section 11, Computer Code for Attri-Edgar Method.

A similar study should be performed for flexible (that is, strain) bus systems.

CONTENTS

LIST OF FIGURES

LIST OF TABLES

1
INTRODUCTION

With the introduction of distributed generation (DG) to the utility industry, the power throughput requirements of substations have risen dramatically. As a consequence, the fault current levels in substation bus work have also increased significantly. The potential now exists for substation short-circuit (SC) current levels to reach as high as 100 kA [8]. Such high SC current levels are of concern to substation designers because the electromagnetic (EM) fields that they generate can interact in ways that produce potentially damaging mechanical forces on bus structural elements.

In order to account for the presence of these mechanical forces during substation design, the IEEE has issued standards [2][3] that provide simple formulas for predicting the maximum static, mechanical force due to SC currents on each span of both rigid, and flexible busbar systems. When specifying insulator cantilever force requirements under short circuit conditions, it is common industry practice to simply use the SC force equations in IEEE Std. 605 with an overload factor of 1. This approach is widely accepted as resulting in bus designs that are overly conservative for the levels of SC current that are anticipated. With the increasing cost of new substation construction and existing station retrofit, there is renewed interest in alternative SC force/stress calculation methods to that of IEEE Std. 605 that are less conservative.

This report documents a study to re-evaluate the applicability of IEEE Std. 605's SC force calculations for rigid bus structures under the conditions of high fault current. The report also identifies an alternative method to that of IEEE Std. 605 which accounts for the effects of bus dynamic response, which represents how the SC forces between the bus conductors is transmitted to the supporting structure. Ideally the force is transmitted instantaneously but modeling the dynamic response includes the tendency of the supports to filter out the SC forcing. Based on this new method, a simple, computerized, SC force calculation tool that substation designers can use to determine realistic SC force assessments is included in this report.

Section 2 provides a brief description of the IEEE Std. 605 methodology highlighting the differences in SC force formulations between IEEE Std. 605-1998 and IEEE Std. 605-2008.

Section 3 addresses the question concerning the continued applicability of IEEE Std. 605 algorithms under conditions of elevated fault current. This is done by building an electromagnetic (EM) force FEA model of a realistic, three-phase, rigid bus structure and comparing the model's SC force predictions to those of the IEEE Std. 605 methodology at both low and high fault current levels.

Section 4 presents three alternative SC force calculation methods to IEEE Std. 605. Two of these three alternative methods are further comprised of two related, but distinct approaches. As a result, a total of five alternative SC force calculation methods are described in this section. In addition to the static response, already modeled by IEEE Std. 605, these methods add a factor that accounts for the dynamic response of a bus structure to an electrical fault, This dynamic factor is a function of the ratio between the natural frequency of the bus structure, and forcing frequency of the electrical short-circuit current. Including bus dynamics in the calculation of SC

force yields more realistic (i.e., less conservative) force predictions. Less "over-engineering" of the bus structure results, which in-turn, contributes toward lower design costs.

Section 5 describes a comparative performance assessment of the IEEE Std. 605 and dynamic SC force prediction methods. This assessment involved coding the three dynamic response methodologies in MATLAB, running the MATLAB routines for a number of SC force case study structures described in the open literature, and comparing the resulting force predictions. The CIGRE Structure D example in Annex F of IEEE Std. 605-2008 [3] is one of the bus structures employed in this study. The tabulated results of this assessment were then analyzed and conclusions were drawn concerning the preferred SC dynamic response method.

Section 6 presents the conclusions and recommendations from the study.

Section 8 provides details of the comparative performance assessment of Section 6 in the form of plots and tables.

Section 9 gives a complete description of the empirical data used in the comparative performance assessment.

A description of a published comparison of advanced SC force prediction methods is provided in Section 10. This research shows that, over a limited scope of bus configuration, FEA is not significantly more accurate than more simplified calculation methods such as the Attri and Edgar's Dynamic Stress Model for Bus Supports.

Finally, the MATLAB routine for the preferred SC dynamic response method was developed into a SC force prediction tool for substation designers. The complete MATLAB code for the tool is provided in Section 11 – Computer Code for Attri-Edgar Method.

2

IEEE STD. 605 - GUIDELINES FOR THE CALCULATION OF SHORT CIRCUIT FORCE IN SUBSTATION RIGID BUSBAR SYSTEMS

General

The overall effort to develop improved substation SC force calculation tools is multifaceted. Ultimately, it will require performing detailed finite element analysis (FEA) modeling of several common bus types and configurations (e.g., rigid/strain bus, vertical/horizontal bus, round/square conductor, etc.) to predict the electromagnetic (EM) forces within the systems, as well as the mechanical responses of bus conductors, insulators, and supporting structures to those EM forces. Model outputs will need to be provided according to industry-standard substation design metrics (e.g., maximum span length/conductor deflection, maximum bending stress/cantilever force, etc.).

A specific research question addressed in this study is whether IEEE Std. 605's guidelines for calculating short circuit forces on substation bus work are still applicable under the new paradigm of higher levels of substation fault current. In order to answer this question, an EM force FEA model was developed for the prediction of SC force between conductors of a three-phase, horizontally-arrayed, rigid busbar system. The mechanical response of the bus conductors or bus support structure was not included in this initial FEA model. The scope of this initial study was limited to the use of this model to cases where automatic fault reclosing, the effects of non-simultaneous faults, the use of busbar damping wires, and the presence of mid-span conductor welds were not considered. Section 3 describes the model development, its validation, and its use in answering the research question at hand.

Overview of IEEE Std. 605 Methodology

The IEEE Standard 605's approach to considering the effects of short circuit forces on the bus conductor and insulators is described in the following steps:

1. Calculate the peak short circuit force, [N/m or lbf/ft]

2. Calculate the cantilever force on the insulator using peak SC force

3. Calculate the maximum allowable span length given the peak SC force and the yield limit of the conductor

Peak Short Circuit Force

In clause 11.3, short circuit loads, of IEEE Std. 605-2008 there is a description of the fundamental physics, namely the application of the Biot-Savart Law, behind the short circuit force calculation. Section 11.3.3.1 provides a basic force equation for infinitely long parallel conductors, which is the simplest case to analyze. The equation assumes that the fault is initiated to produce the maximum asymmetrical (i.e. current with DC offset) current. The standard

indicates this specifically means that the peak asymmetrical current is $2\sqrt{2}$ times the RMS symmetrical current. The ratio of the peak asymmetrical current to the RMS symmetrical current is known as K in the IEEE Standards. It is tabulated for a range of X/R (i.e. the ratio of the system Thévenin equivalent reactance to the system Thévenin equivalent resistance) from 1 to 1000 where $2\sqrt{2}$ corresponds to an infinite X/R [8]. The force per unit length in N/m is calculated with the following equation

$$F_{SC} = \frac{16\Gamma I_{SC}^2}{10^7 D}$$

(1.1)

where

I_{SC} = the symmetrical RMS fault current, [A RMS],

D = the conductor spacing from center to center, [m], and

Γ = a constant based on the type of fault, the conductor arrangement and the conductor on which the force is applied.

It is clear when considering a line-to-line fault or a single-phase fault with Γ equal to 1 that this equation comes from the textbook equation given below for infinite parallel conductors [10]:

$$|F_1| = \frac{\mu_0 I_1 I_2}{2\pi d}$$

(1.2)

where

I_1 = current in parallel conductor one,

I_2 = current in parallel conductor two,

d = distance between conductors.

$$I_1 = I_2 = 2\sqrt{2} * I_{SC}$$

(1.3)

$$d = D$$

(1.4)

$$\mu_0 = 4\pi * 10^{-7} \frac{H}{m}$$

(1.5)

The value of Γ is summarized in Figure 2-1 below, which is Table 13 in IEEE Std. 605-2008 [3].

Type of short circuit	Configuration	Conductor	Γ
Phase to phase	A, B spaced by D	A or B	1.000
Three phase	A, B, C spaced by D and D	B	0.866
Three phase	A, B, C spaced by D and D	A or C	0.808
Phase to phase	Triangular arrangement—equilateral triangle—side D	A or B	1.0
Three phase	Triangular arrangement—equilateral triangle—side D	A or B or C	0.5
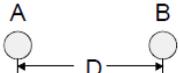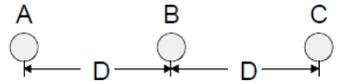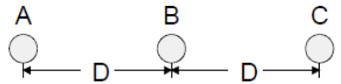
NOTE—For a three-phase fault, this table indicates that the maximum force is on the central conductor B. However, results from finite-element calculations (which provide a much closer estimation of the maximum forces than the preceding equation) indicate that in most cases, the maximum stresses and transmitted effects on the support structure are in either conductor A or C.

Figure 2-1
Constant for Short Circuit Basic Force Equation from IEEE Std. 605-2008 [3]

The equation presented in section 11.3.3.1 of IEEE Std. 605-2008 is based on the following simplifying assumptions:

1. The conductor length is infinite. This ignores the end effects that factor into the evaluation of complex bus structures.

2. The peak asymmetrical current level is twice the level of the peak symmetrical current. In practice, the peak asymmetrical current is a function of the time constant of the circuit. In order to account for this momentary peak factor effect, the standard proposes a correction factor called the *half-cycle decrement factor*, D_f, which is defined below.

3. The bus support structure responds instep with the forcing function (i.e. the electromagnetic force). Experimental tests have shown that the maximum response of the bus (i.e. deflection) and the peak of the fault current do not coincide. This is because the natural frequency of the combined bus and support structure is typically much smaller than that of the forcing function (i.e. electrical short-circuit current).

4. Damping of the bus and its support structure can be ignored. Damping wires are added to rigid bus work to reduce its dynamic response to the 60 Hz forcing function of fault current. The addition of the wire's mass to that of the busbar lowers the overall bus structure's natural frequency. This in turn, raises the level of SC force at which bus damage occurs. In order to reduce the conservatism of IEEE Std. 605 SC force calculations, the effect of adding the damping wire's mass on the natural frequency and the effect of the dynamic response on support cantilever force should be included in the analysis.

5. During three-phase faults, the peak electromagnetic force occurs at the moment of peak asymmetric current. Attri and Edgar show that moment-maximum force occurs 180 degrees after fault inception, which occurs after the current peak on the middle conductor and before the peak on one of the outer conductors [4].

6. The peak electromagnetic force on the middle conductor is the largest. The analysis of Attri and Edgar show that peak support cantilever force and conductor bending stress occur in general on one of the middle conductor to the dynamic response of the bus assembly.

In response to the conservatism from the previous assumptions, section 11.3.3.2 of IEEE Std. 605-2008 proposes the following corrected, short circuit force equation:

$$F_{SC\_corrected} = D_f^2 K_f F_{SC} \qquad (1.6)$$

where

D_f = the half-cycle decrement factor,

K_f = the structure flexibility factor.

The half-cycle decrement factor corrects for the assumption that the fault current is fully offset and is given by the following equations.

$$T_a = \frac{X}{R} \frac{1}{2\pi f} \qquad (1.7)$$

$$D_f = \frac{1 + e^{-\frac{1}{2fT_a}}}{2} \qquad (1.8)$$

It is important to note that D_f is really the maximum half-cycle decrement factor since it corrects the calculation from the peak asymmetric current only. Additional correction or current decrement is needed beyond the first half-cycle (i.e. as the fault continues and the offset decays).

The effect of support structure flexibility is accounted for by the mounting-structure flexibility factor, K_f. The value of K_f is summarized for single-phase supports in Figure 2-2, which is Figure 20 borrowed from IEEE Std. 605-2008 [3]. K_f is unity for three-phase supports. K_f is the only factor that provides a reduction in conservatism related to the bus structure.

Bus Height (ft)
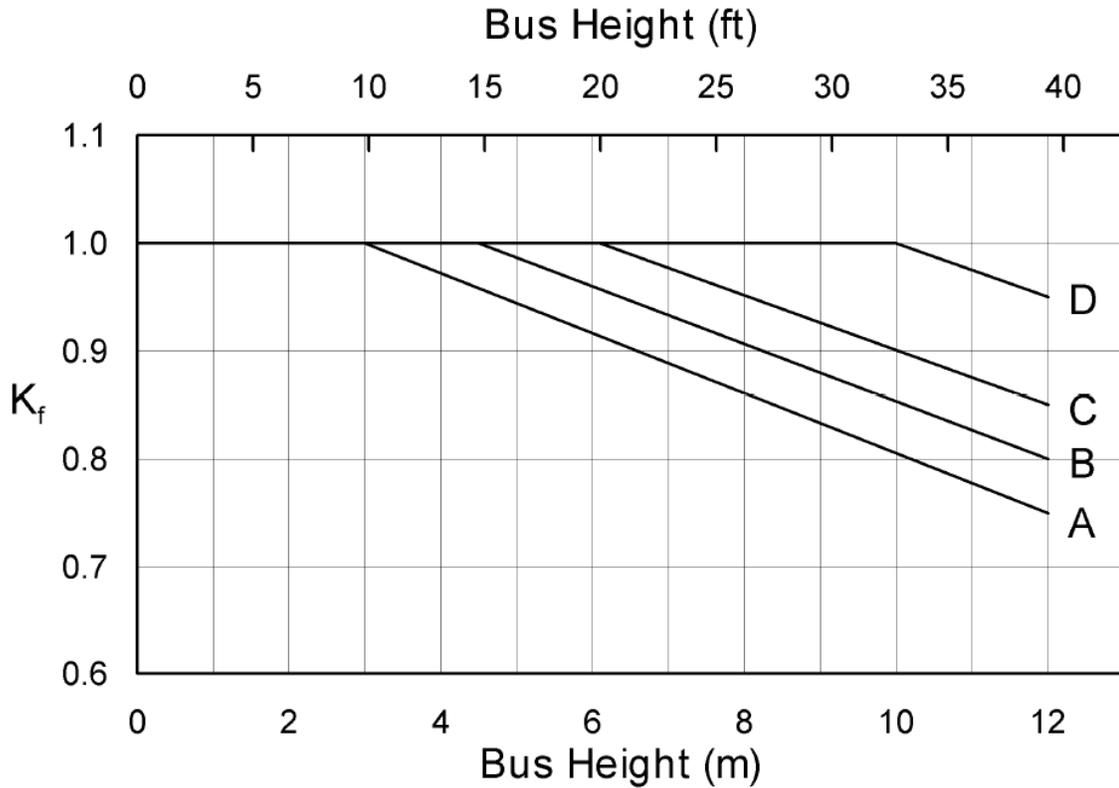
NOTE—A, lattice and tubular aluminum; B, tubular and wide-flange steel and wood pole; C, lattice steel; D, solid concrete.

Figure 2-2
Mounting-structure Flexibility Factor for IEEE Std. 605-2008 [3]

The corrected short circuit force for IEEE Std. 605-1998 is provided below for completeness since one of the dynamic methods utilizes the 1998 version of the standard. F_{SC_1998} is the corrected short circuit force in lbf/ft.

$$F_{SC\_1998} = \frac{C\,\Gamma\,(D_f\,\sqrt{2}\,I_{SC})^2}{D} \tag{1.9}$$

$$D_f = \sqrt{1 + \frac{T_a}{t_f}(1 - e^{-\frac{2t_f}{T_a}})} \tag{1.10}$$

where

$C = 5.4*10^{-7}$,

D = the conductor spacing from center to center, [in] and

t_f = the short circuit duration, [s].

Short Circuit Induced Insulator Cantilever Force

The cantilever force that is applied to the top of the insulator is calculated according to [3] as follows:

$$F_{scC} = F_{SC} L_e \tag{1.11}$$

where

F_{scC} = is the short circuit cantilever force, [N, lbf] and

L_e = the effective conductor span length, [m, ft].

Bus configuration	Support (boundary) conditions					Maximum span length L_E
	S1	S2	S3	S4	S5	
Single-span	P	P				L/2
Single-span	P	F				5 L/8 (Max at S2)
Single-span	F	F				L/2
Two Cont.-span	P	C	P			5 L/4 (Max at S2)
Two Cont.-span	P	F	F			9L/8 (Max at S2)
Two Cont.-span	F	F	F			L (Max at S2)
Three Cont.-span	P	C	C	P		11 L/10 (Max at S2)
Four Cont.-span	P	C	C	C	P	8 L/7 (Max at S2)

where

    L   is the bus span between supports (assumed equal between all supports)
    P   is for pinned-end condition at the support
    F   is for fixed-end condition at the support
    C   is for mid-support condition of continuous span

NOTE—This table is applicable only to equal-span bus arrangement. The mid-support of a continuous bus has only reaction force resistance but no moment resistance, although the continuous bus conductor connected to it has a moment. For continuous spans of more than the spans shown, use the value of L_E for the largest span shown for the same end conditions.

Figure 2-3
Maximum effective span length for IEEE Std. 605-2008 [3]

Maximum Allowable Span Length

The maximum allowable span length is calculated for IEEE Std. 605-2008 as follows for a single span bus arrangement:

$$L_S = \sqrt{\frac{A J \sigma_{allowable}}{F_T D_o}} \tag{1.12}$$

where

L_S = is the maximum allowable span based on the maximum fiber stress, [m, in]

$\sigma_{allowable}$ = is the allowable conductor bending stress, [Pa, psi],

J = is the conductor bending moment of inertia, [m^4, in^4],

F_T = is the total force acting on the conductor per unit length, [N/m, lbf/ft],

D_o = is the conductor outside diameter, [m, in].

A = is a factor that depends on the end conditions. See Table 2-1.

The maximum allowable span length is calculated for IEEE Std. 605-1998 as follows for a single and multi-span bus arrangement:

$$L_S = C \sqrt{\frac{A F_A S}{F_T}}$$ (1.13)

where

L_S = is the maximum allowable span based on the maximum fiber stress, [cm, in]

C = is 3.16 for Metric units and 3.46 for English units,

F_A = is the allowable conductor bending stress, [kPa, psi],

S= is the conductor section modulus, [cm^3, in^3],

F_T = is the total force acting on the conductor per unit length, [N/m, lbf/ft],

A = is a factor that depends on the end conditions and the number of spans. See Table 2-1.

Table 2-1
Factor for maximum allowable span calculation [2]-[3]

Span length / end conditions	IEEE Std. 605-2008	IEEE Std. 605-1998
1 / pinned-pinned	16	8
1 / pinned-fixed	16	8
1/ fixed-fixed	24	12
2 / continuous bus	-	8
3 / continuous bus	-	10
4 / continuous bus	-	28

3
EM FORCE FEA MODEL OF RIGID BUSBAR

Model Description

The FEA model employed in this study was implemented using the COMSOL Multiphysics 4.2a software package. It consists of two coupled sub-models: an electric circuit of the Thévenin equivalent of the system source and a finite element model of the busbar. The electric circuit determines the current density in the busbar whereas the finite element sub-model calculates the magnetic field and the forces in the busbar. The FEA can be two-way coupled, i.e. the finite element sub-model correctly simulates the voltage drop along the busbar at any instance of time, which can be fed into the electric circuit sub-model if required.

The electric circuit (Figure 3-1) contains the lumped elements of the simulation model. In the most basic case it consists of a three-phase voltage source V_S, series inductances L_S, series resistances R_S, and load resistances R_L. Ideal switches are added to simulate the fault. A three-phase-to-ground fault is represented by closing all three switches named S_{Fa} whereas a floating line-to-line fault can be implemented by closing S_{Fb}. Additionally, a single line-to-ground fault can be achieved by closing one of the S_{Fa} switches. More sophisticated models of transmission lines and power transformers could be added as required.

The finite element sub-model was implemented as a two-dimensional geometry (Figure 3-2). This is valid as long as there is no geometric variation along the length of the busbar. The busbars were considered to be hollow tubes of circular shape made from aluminum. The length of the busbar structure only matters if two-way coupling between the FEA and the circuit model is required. It is provided as a separate number in the equation settings of COMSOL. Special care should be taken that a fully-transient implementation of Ampère's circuital law is chosen. The time resolution needs to be fine enough to assure a good reading of the maximum peak currents and forces. A time resolution of 0.2 to 1.0 ms is a reasonable choice for typical power frequencies of 50 Hz or 60 Hz. The simulation runs until symmetrical currents are obtained.

Figure 3-3 shows the electric current for each phase of the three phase bus. The line-to-line source voltage was 266 kV$_{RMS}$ at 60 Hz power frequency. The source inductance and source resistance are 5 mH and 1.9 mΩ, respectively. The X/R ratio on the source side is approximately 1000. The load resistance is 50 Ω resulting in a load current of 3.1 kA$_{RMS}$. The asymmetric peak value of the short circuit current depends on the exact point-on-wave when the fault occurs. Therefore, it is important to close the switch at the correct moment in time. In order to have the peak offset, the fault is chosen to occur at t = 31 ms in the case of a three-phase fault. The maximum peak current is 223 kA$_{Peak}$. After approximately four seconds, it approaches a symmetrical (steady state) fault current of 80 kA$_{RMS}$. This results in a maximum peak force of 3140 N/m (Figure 3-4). The forces in the three busbars sum up to zero at any instant of time.
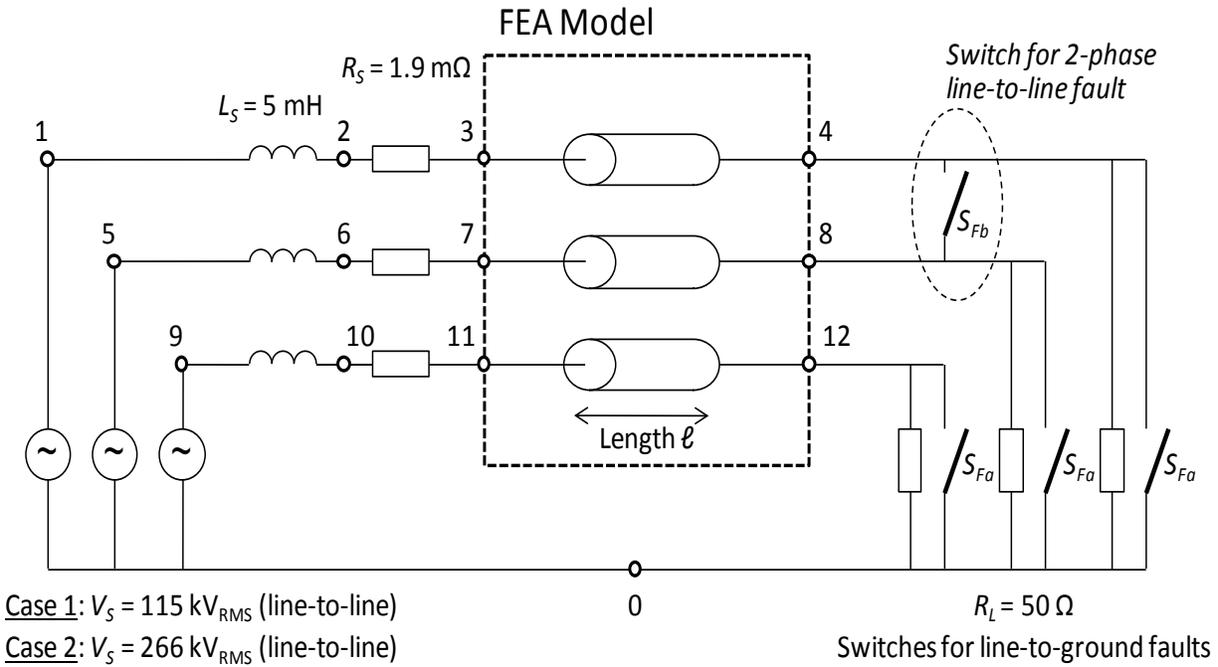
Figure 3-1
FEA Model: Three-Phase Electric Circuit. The Node Numbers Correspond to the Particular Implementation Based on a SPICE Netlist
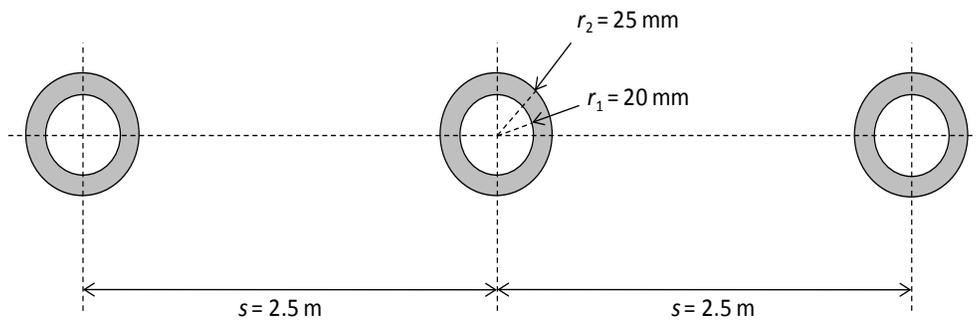
Figure 3-2
FEA Model: Two-Dimensional Geometry of the FEA Model
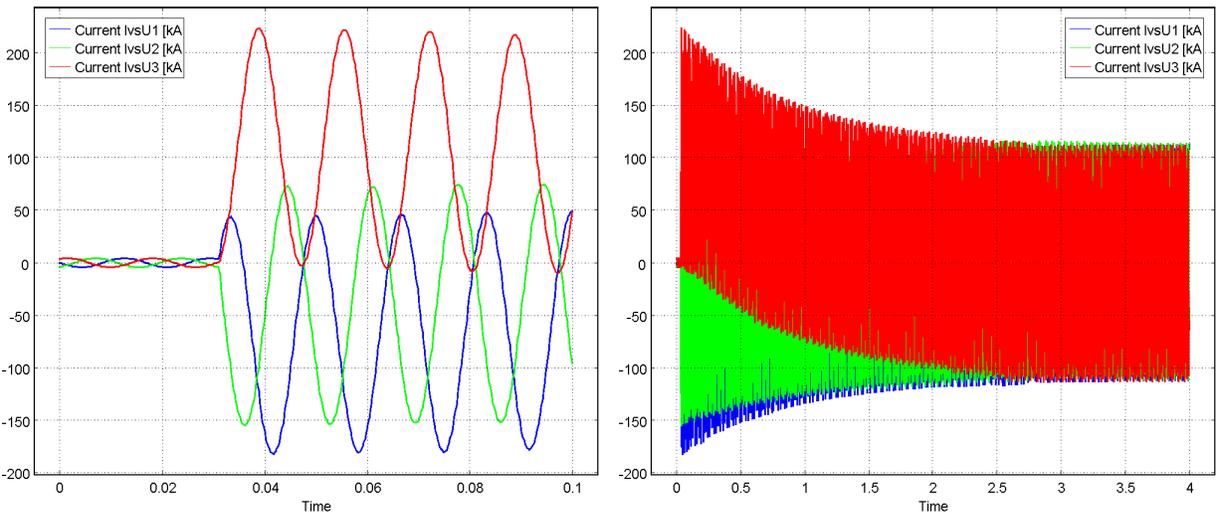
Figure 3-3
FEA Model: Currents in the Three Busbars for the First 100 ms (Left) and for the Full Run of 4 s (Right)
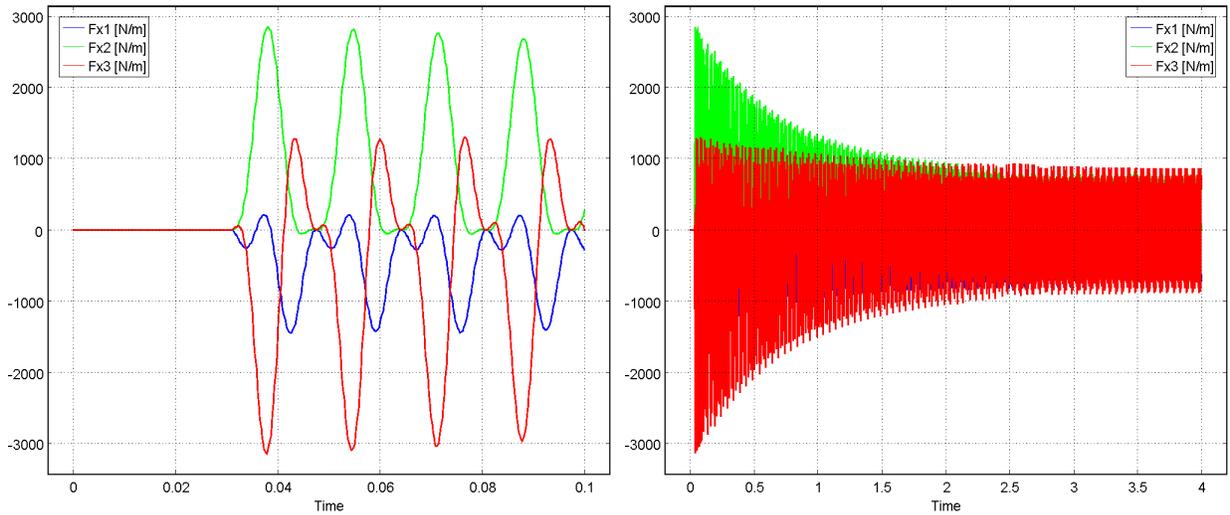
Figure 3-4
FEA Model: Forces per Meter Length Acting on Each of the Three Busbars for the First 100 ms (Left) and for the Full Run of 4 s (Right)

FEA Model Validation

It is essential to validate the EM force FEA before making use of it. The simple geometry of the horizontal bus affords the use of simpler methods such as hand calculation or a transient power system network solver. Case #2 will be considered in the validation, which corresponds to a source line-to-line voltage of 266 kV with corresponding SC current and force plots shown in

Figure 3-3 and Figure 3-4. The symmetrical RMS fault current can be calculated as the ratio of the source voltage to the source impedance.

$$I_{sym,RMS} = \frac{V_{L-L}}{\sqrt{3}} \frac{1}{Z} \tag{2.1}$$

The calculated symmetrical RMS current is 81.5 kA. The asymmetrical peak can then be found by multiplying the symmetrical RMS current by the asymmetry factor, K as shown below.

$$I_{asym,pk} = K * I_{sym,RMS} \tag{2.2}$$

K depends on the ratio of source reactance to the source resistance (i.e. X/R). Table 17 of [8] has values for K for X/R values ranging 1 to 1000. The case to be considered has an X/R of 1000, which corresponds to a value of K of 2.824. The calculated peak asymmetric current is then calculated to be 230.1 kA. The peak force between conductors (i.e. for example, between phase A and phase B) can then be estimated with the following equation assuming that the peak currents are known.

$$|F_{ab}| = \frac{\mu_0 I_{a,pk} I_{b,pk}}{2\pi d} \tag{2.3}$$

Since there are no simple factors relating the symmetrical RMS value to the asymmetric value of the outer phases (i.e. A and C) at the time of peak offset, a hand calculation can be challenging. Another problem associated with a simple hand calculation is that the peak force does not correspond to the peak of the current as shown by Attri and Edgar [4]. PSCAD/EMTDC has therefore been employed for more accurate calculation of the short circuit currents and the resulting forces. The results are shown in Figure 3-5 and Figure 3-6 as well as in Table 3-1 and Table 3-2. These results show that the peak forces experienced by the middle conductor and by one of the outer conductors deviate between 2% and 8% in difference as calculated by the EM force FEA and the PSCAD/EMTDC model.
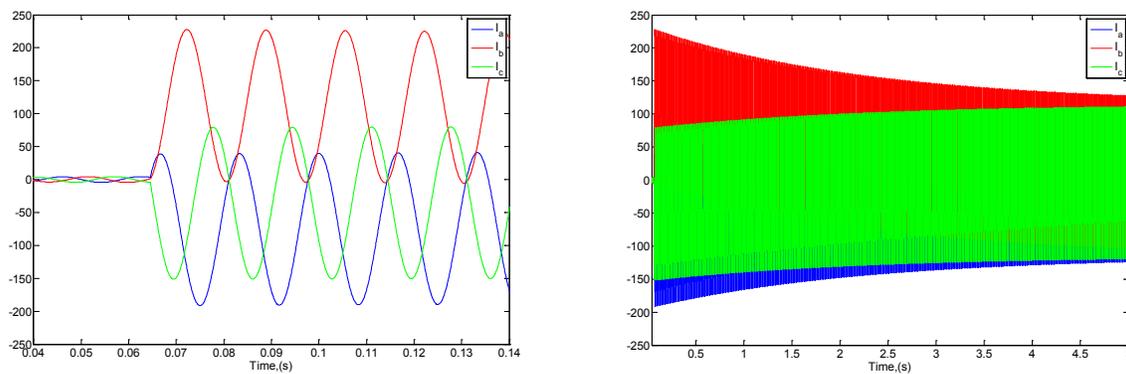
Figure 3-5
PSCAD/EMTDC Model: Currents in the Three Busbars for the First 100 ms (Left) and for the Full Run of 5 s (Right)
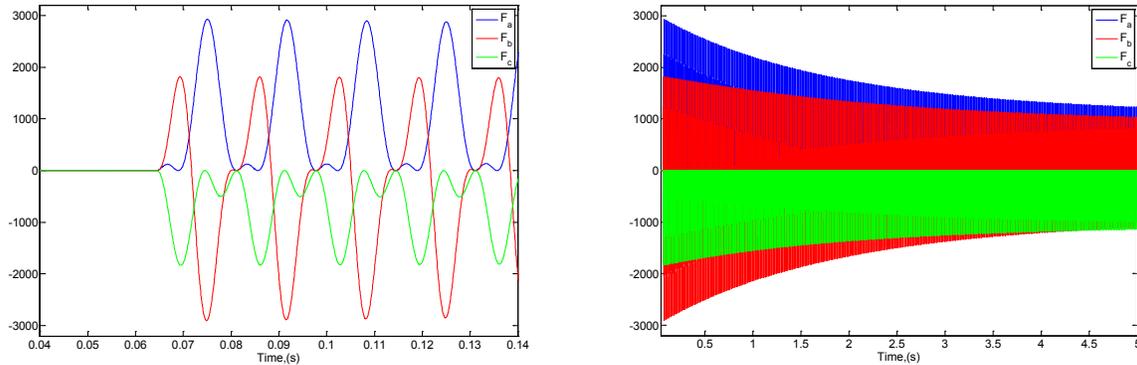
Figure 3-6
PSCAD/EMTDC Model: Forces per Meter Length Acting on Each of the Three Busbars for the First 100 ms (Left) and for the Full Run of 5 s (Right)

Table 3-1
Peak Forces Acting on the Busbar: Comparison of FEA Results with PSCAD/EMTDC

	Max. Force FEA Model [N/m]			Max. Force PSCAD/EMTDC [N/m]			Difference
3 phase ~80 kA$_{RMS}$	1440	3140	2850	2928	2903	1835	2%-8%

Comparison of IEEE Std. 605 SC Force Calculation to EM Force FEA

Table 3-2 summarizes the simulation results from the FEA model for 2-phase ungrounded and 3-phase grounded faults and compares them with calculated forces from IEEE Standard 605. The lower fault currents refer to 115 kV system voltage ("Case 1" in Figure 3-1) and the higher fault currents were obtained with 266 kV system voltage ("Case 2").

Table 3-2
Peak Forces Acting on the Busbar: Comparison of FEA Results with IEEE Std. 605-2008

	Max. Force FEA Model [N/m]			Max. Force IEEE 605 [N/m]			Difference
3 phase 35 kA$_{RMS}$	269	608	552	632	677	632	11.4% for phase B
2 phase 30 kA$_{RMS}$	6.3	505	496	−	574	574	13.7% for phase B
3 phase 80 kA$_{RMS}$	1440	3140	2850	3299	3536	3299	12.6% for phase B
2 phase 70 kA$_{RMS}$	35	2940	2900	−	3126	3126	6.3% for phase B

All force values provided for the FEA are estimated to have an error margin of approximately ±3%. The accuracy is limited mainly due to the simulation time step of 0.2 s. Regarding the IEEE Std. 605 SC force calculation, the half-cycle decrement factor was calculated based on the system impedance modeled in the FEA. The flexibility factor has been assumed to be unity. It should be noted also that the symmetrical RMS current found by the FEA was utilized in the IEEE Std. 605 calculations. The FEA model provided slightly lower maximum force values in comparison to the force values calculated by IEEE Std. 605. The conservatism in the IEEE Std. 605 peak SC force calculation appears to be consistent with increased fault current levels.

4
DYNAMIC RESPONSE PREDICTION

Typical industry practice concerning the design of rigid busbar systems is to use the IEEE Std. 605 calculation of peak, static SC force described in Section 1 without consideration of bus system dynamic response [8]. As was noted in earlier sections of this report, such an approach yields overly conservative bus system designs (e.g., insulators are sized by a SC force overload factor of 1.0). This is conservative because the relatively low natural frequencies of typical bus structures cause them to be insensitive to the 60-cycle and 120-cycle components of the force [4]. As a result, the natural response to the second research question addressed in this study as to how IEEE Std. 605's SC force calculation methodology can be improved, is to include bus dynamic response in the determination of required dynamic design force. This section describes several approaches proposed in the open literature for bringing bus dynamics into the determination of this required design force.

IEC Std. 865-1

IEC 865-1 [6] provides a methodology for determining the impact of SC current mechanical force on rigid busbars and their supports that includes consideration of bus dynamics through the application of correction factors to the static SC force calculation. The factors depend on whether the simplified or detailed method is used. It should be noted that on page 35 in the section of the standard describing the method's frequency-dependent factors, "NOTES 1", it states that, "Short-circuit duration $T_k \leq 0.1$ s can cause an appreciable reduction of the stress in structures with $f_c/f \leq 1$" [6]. This comment reinforces a principal assertion of this report that consideration of bus dynamic response to short circuit forcing function can provide significant reductions in the conservatism of SC current force predictions.

The IEC 865-1 approach calculates the maximum short circuit static force for a SC between three (or two conductors) of a three-phase, rigid bus system in a fashion similar to that of IEEE Std. 605.

$$F_{m3} = \frac{\mu_0}{2\pi} \frac{\sqrt{3}}{2} i_{p3}^2 \frac{l}{a_m} \tag{3.1}$$

$$i_{p3} = \sqrt{2}\, \kappa\, i_{k3}'' \tag{3.2}$$

$$F_{m2} = \frac{\mu_0}{2\pi} i_{p2}^2 \frac{l}{a_m} \tag{3.3}$$

$$i_{p2} = \sqrt{2}\, \kappa\, i_{k2}'' \tag{3.4}$$

where

F_{m3}= the force on the central main conductor during a balanced three-phase short circuit, [N]

F_{m2}= the force between main conductors during a line-to-line short circuit, [N]

a_m = the effective distance between neighboring conductors, [m],

l = the span length, [m],

κ = the factor for the calculation of peak short circuit current,

i_{p3} = the peak short circuit current in case of a balanced three-phase short circuit [A],

i_{k3}'' = the three-phase initial symmetrical short circuit current, [A RMS],

i_{p2} = the peak short circuit current in case of a line-to-line short circuit,

i_{k2}'' = the line-to-line initial symmetrical short circuit current, [A RMS].

Simplified Method Dynamic Factors

The simplified method provides an estimation of the dynamic factors without knowledge of the bus assembly natural frequency. Only a few quantities need to be known or calculated to calculate all of the dynamic factors:

1. The minimum conductor yield strength, [MPa]

2. The calculated conductor bending stress, [MPa]

Figure 4-1 and Figure 4-2 show the dynamic factors for line-to-line and three-phase faults, respectively.
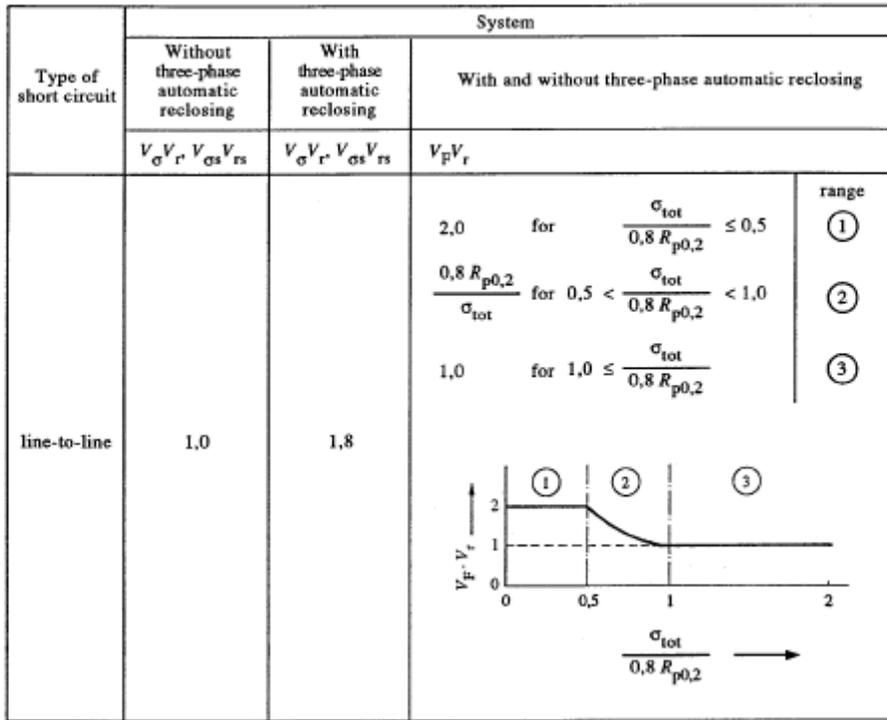
Figure 4-1
Simplified Method's Dynamic Response Factors for Line-to-Line Faults [6]

three-phase	1,0	1,8	$2{,}7$ for $\dfrac{\sigma_{tot}}{0{,}8\,R_{p0,2}} \le 0{,}370$ — range ① $\dfrac{0{,}8\,R_{p0,2}}{\sigma_{tot}}$ for $0{,}370 < \dfrac{\sigma_{tot}}{0{,}8\,R_{p0,2}} < 1{,}0$ — range ② $1{,}0$ for $1{,}0 \le \dfrac{\sigma_{tot}}{0{,}8\,R_{p0,2}}$ — range ③
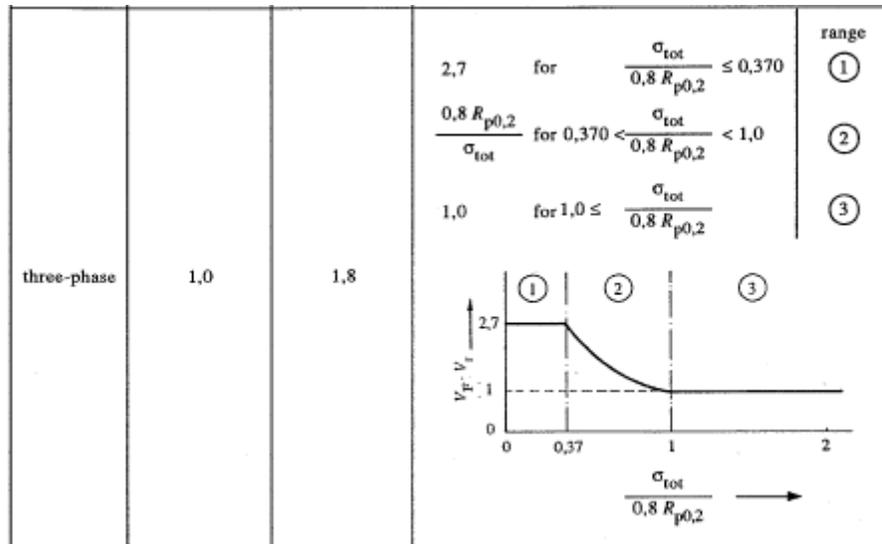
Figure 4-2
Simplified Method's Dynamic Response Factors for Three-phase Faults [6]

Detailed Method Dynamic Factors

These factors are each functions of the ratio of bus natural frequency (f_c) to the system electrical frequency (f) (i.e., f_c/f) as shown in Figure 4-3 through Figure 4-5. Figure 4-3 and Figure 4-4 have multiple curves corresponding to different amount of asymmetry represented by a value of κ. The factors were derived and validated with extensive modeling and comparisons with experimental values [11]. Figure 4-3 represents the ratio of the calculated dynamic force to the calculated static force over a range of frequencies. It can be thought of as frequency response of the bus conductor and its supports to the SC forcing. If the ratio of the mechanical system (i.e. the bus and its support structure) frequency is low compared to the forcing frequency of the electric power system, then the response is attenuated and the factor is below 1. As the ratio starts to increase towards unity, however, the response rises to a peak at the resonant value of $f_c/f = 1$. The peak between values of f_c/f of 0.8 and 1.3 is flat due to logarithmic damping. There is a second peak for three-phase faults that corresponds to the 2nd resonant point. The companion book to CIGRE brochure 105 does not explicitly state why there is peak at $f_c/f = 2$ for line-to-line faults. The suspected reason is that the steady-state double-frequency oscillations are twice as large for the middle conductor in a three-phase fault than for the conductors in a line-to-line fault [11]. Figure 4-6 and Figure 4-7 shows curves for calculated values (solid and small dashed curves) with the standardized curve (large dashed curve). Note the resonant peaks in the calculated values.
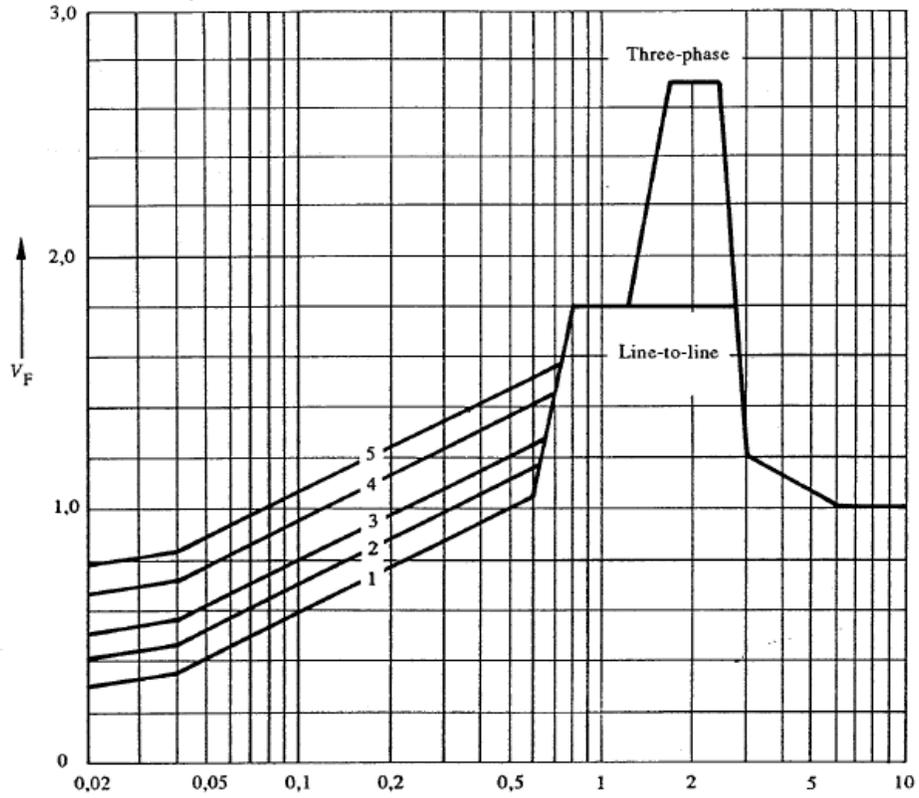
Figure 4-3
Detailed Method Support Dynamic Factor, V_F [6]

$$\frac{f_e}{f} \text{ or } \frac{f_{cs}}{f} \longrightarrow$$

IEC 1 036/93

1 $\kappa \geq 1,60$	2 $\kappa = 1,40$	3 $\kappa = 1,25$
4 $\kappa = 1,10$	5 $\kappa = 1,00$	
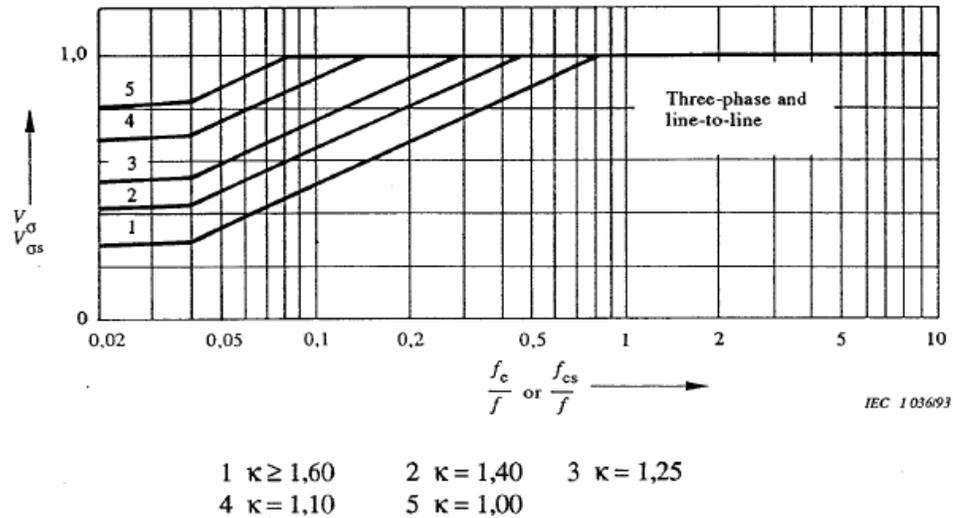
Figure 4-4
Detailed Method Conductor Bending Stress Dynamic Factor, V_σ [6]
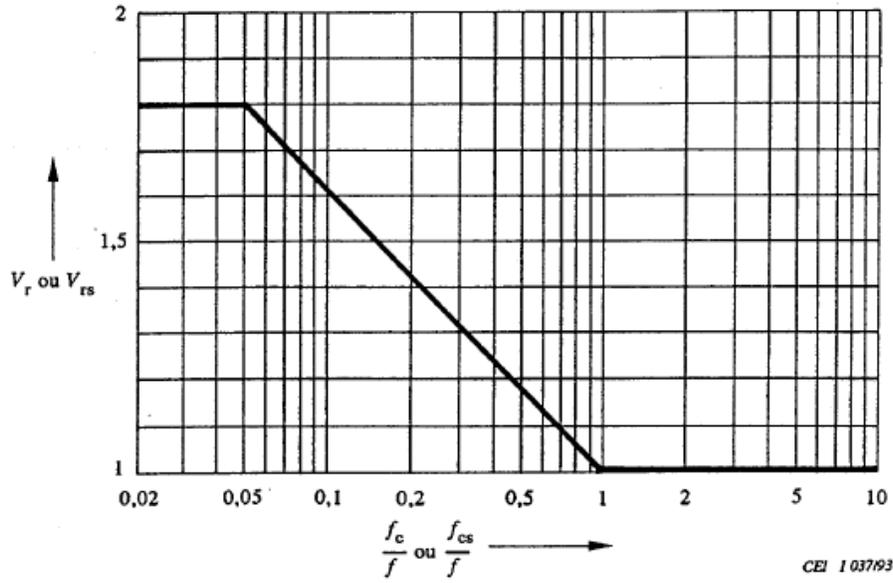
Figure 4-5
Detailed Method Autoreclosure Dynamic Factor, V$_r$ [6]
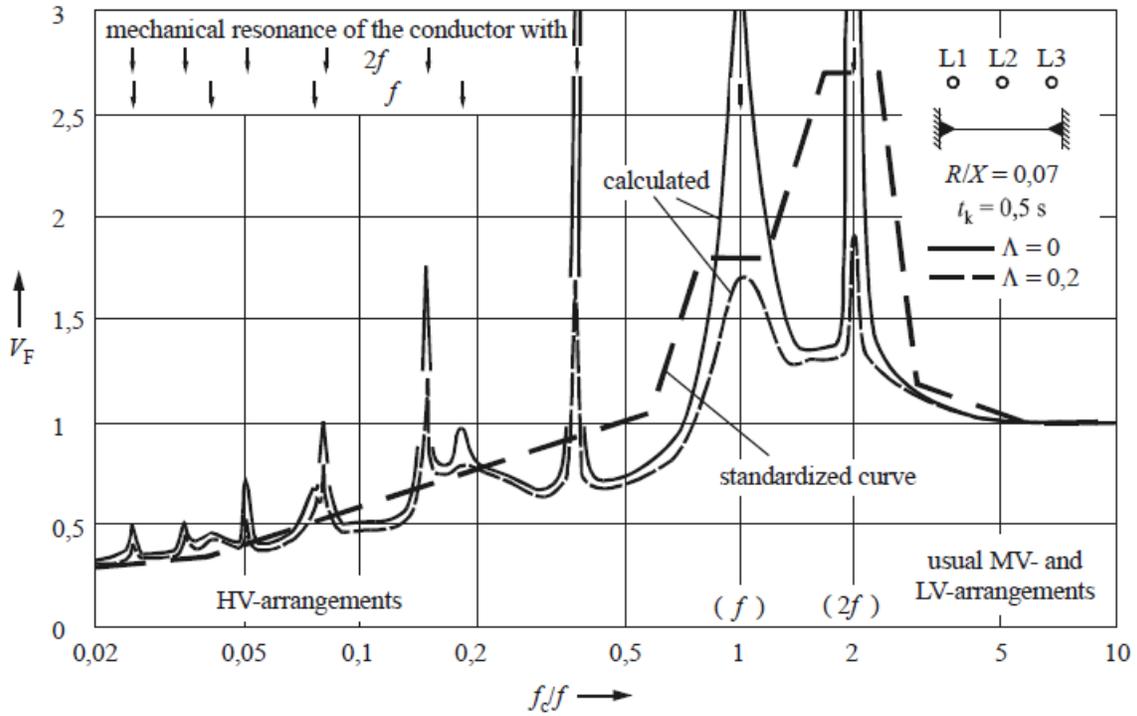
Figure 4-6
Calculated Dynamic Factor, V$_F$, Curves with IEC 865-1 Standardized Curve [11]
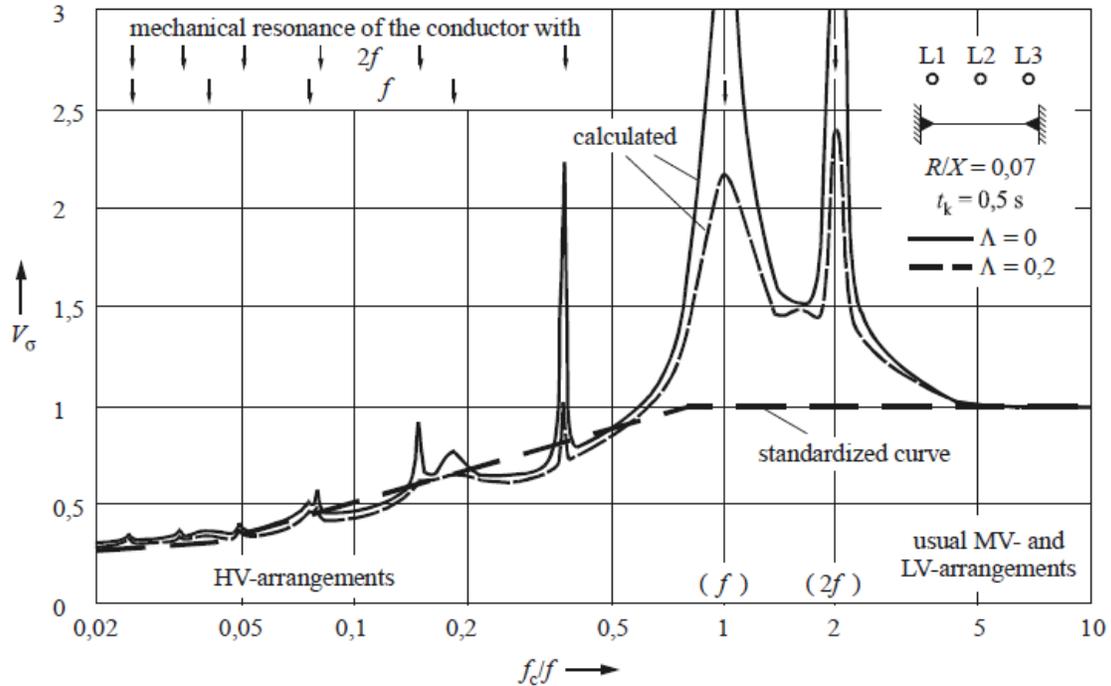
Figure 4-7
Calculated Dynamic Factor, V_σ, Curves with IEC 865-1 Standardized Curve [11]

Bus Natural Frequency

The calculation of conductor's natural frequency is computed as follows:

$$f_c = \frac{\gamma}{l^2}\sqrt{\frac{EJ}{m'}} \tag{3.5}$$

where

f_c= main conductor natural frequency, [Hz],

γ = factor depending on end conditions of beam (i.e. main conductor) (see Figure 4-8),

E = the modulus of elasticity of main conductor, [Pa]

J = the second moment of area of main conductor, [m^4]

m' = the mass per unit length of main conductor, [kg/m].

Bus Conductor Design

From the maximum static force, F_m, the bending stress on the conductor (σ_{tot}) is determined using the following formula:

$$\sigma_{tot} = V_\sigma V_r \beta \frac{F_m l}{8Z} \tag{3.6}$$

where

F_m = either F_{m2} or F_{m3} depending if line-to-line or three-phase fault, [N],

V_σ = the dynamic factor for conductor bending stress,

V_r = the dynamic factor for autoreclosure,

β = the factor for conductor bending stress,

Z = the section modulus of the main conductor.

This value is compared with the conductor material's yield stress multiplied by a factor q, which accounts for the cross-sectional form of the bus conductor (i.e., solid bar, round tubing, or square tubing). Rigid bus dynamic response is accounted for in the calculation of conductor bending stress by incorporating two empirically-derived correction factors V_σ and V_r.

Bus Insulator Design

The impact of SC forces on bus supports is also evaluated in IEC Std. 865-1 by calculating the maximum dynamic cantilever force, F_d on the top of the support resulting from the interaction of the SC forcing of bus and reaction of the supports. F_d is calculated using empirically-derived factors V_F and V_r. The values for V_r, and V_F based on the type of short circuit (i.e., one phase, line-to-line or three-phase) can be seen in Figure 4-1 through Figure 4-3 and Figure 4-5, which is a copy of Table 2 and Figure 4 from [6]. In order to calculate the cantilever force on the supports, the calculated distributed force has to be concentrated according to the arrangement of the bus support structure. Factors α-A and α-B as shown in Figure 4-8 are used to calculate the cantilever force on the fixed supported and simply supported ends for single spans and the outer support and inner support ends for multiple spans, respectively.

Type of beam and support			Factor α	Factor β*	Factor γ
Single span beam	A and B: simple supports		A: 0,5 B: 0,5	1,0	1,57
	A: fixed support B: simple support		A: 0,625 B: 0,375	0,73	2,45
	A and B: fixed supports		A: 0,5 B: 0,5	0,5	3,56
Continuous beam with equidistant simple supports	Two spans		A: 0,375 B: 1,25	0,73	2,45
	Three or more spans		A: 0,4 B: 1,1	0,73	3,56
* Plasticity effects included					
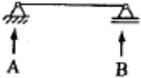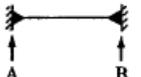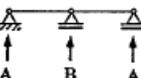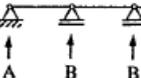
Figure 4-8
Factors for different bus support arrangements [6]

Attri and Edgar's Dynamic Stress Model for Bus Supports

N.S. Attri and R.N. Edgar [4] developed a dynamic stress prediction model for bus supports. The busbar and its support structure are modeled as a simple spring mass system. The masses are located at the supports and they represent the concentrated mass of the bus with the mass of its corresponding insulator. The insulator's elasticity or spring constant is modeled by the springs. The authors derive a natural frequency for the system with the following formula:

$$F\omega = \sqrt{\frac{1}{\sum_{i=1}^{n} M_i} \frac{3\,E\,I\,L}{\sum_{i=1}^{n} \xi_i^2 (L - \xi_i)^2} + \frac{\sum_{i=1}^{n} k_i}{\sum_{i=1}^{n} M_i}} \qquad (3.7)$$

where

ω = the system natural frequency, [rad/s],

E = the bus conductor modulus of elasticity, [Pa],

I = the bus conductor 2nd moment of area, $[m^4]$,

L = the total length of bus conductor, [m],

k_i = the insulator spring constant, [N/m],

M_i = the concentrated mass at the supports, [kg] and

ξ_i = the insulator location along the bus conductor, [m].

The approach is based on the following formula for the maximum static force that bus supports must be designed to withstand during three-phase, and phase-to-phase faults, as adopted by the National Standards for Power Switching Equipment (NEMA) [12]:

Three-phase faults:

$$F = 6.9 \left(\frac{5.4 I_{rms}^2}{10^7 S} \right) \tag{3.8}$$

Phase-to-phase faults:

$$F = 8 \left(\frac{5.4 I_{rms}^2}{10^7 S} \right) \tag{3.9}$$

where

I_{rms} = the symmetrical three-phase, RMS fault current, and

S = the conductor spacing, m.

The following excerpt from Attri and Edgar's paper introduces the methodology employed:

The actual dynamic displacement of each phase of a simple bus structure is derived in Appendix III of [4]. In the case of the middle phase, it is given by

$$y(t) = \left(\frac{5.4 I_{rms}^2}{10^7 Sk} \right) \sqrt{3} \left[\frac{sin(\omega t - \mu_4)}{\sqrt{B}} + \frac{exp\left(-2\frac{R}{L}\right)t}{B} \right] \tag{3.10}$$

where

ω = the natural frequency of simple bus structure, rad/s,

k = the spring constant of a simple bus system, in lb/in,

$\frac{L}{R}$ = the time constant of the power system in seconds

f = the electrical system frequency, in hertz,

$B = \left(\frac{2 R/L}{\omega} \right)^2 + 1$, and

$\mu_4 = tan^{-1} \frac{\omega}{2R/L}$

4-9

Unlike the center phase, the outside phases are subjected to a dc force component due to the steady-state currents. The displacement of outside phase b, which is affected most, is given by

$$y(t) = \left(\frac{5.4 I_{rms}^2}{10^7 Sk}\right)\sqrt{3}\left[0.433(1 - \cos\omega t) + \frac{\sin(\omega t - \mu_4)}{\sqrt{B}} + \frac{exp\left(-2\frac{R}{L}t\right)}{B}\right] \quad (3.11)$$

The maximum possible displacement of outside phase c is much smaller.

The actual required design force for the bus supports is given by the maximum value of the product of $ky(t)$ obtained from the equations above. The magnitude of this design force is affected by the natural frequency of the bus ω and the X/R ratio or time constant L/R of the power system. The required design force may be expressed as

$$ky(t) = H\left(\frac{R}{L}, \omega\right)\left(\frac{5.4 I_{rms}^2}{10^7 S}\right) \quad (3.12)$$

Minimum and maximum values of H are shown in Figure 4-9 . These limits correspond to very small and relatively large values of R/Lω and are independent of the actual magnitude of R/L. The NEMA formula may be modified by a factor N to determine the required design force.

$$F = N \times 6.9 \left(\frac{5.4 I_{rms}^2}{10^7 S}\right) \quad (3.13)$$

If the X/R ratio of the circuit is assumed to be 25, that is R/L= 15, then the factor N may be expressed as a function of R/Lω only as shown in Figure 2 (i.e. Figure 4-10). The factor N in this figure could be applied safely to any design where X/R < 25 which would include most applications. N factors corresponding to other values of X/R may be calculated from the equations given earlier. It is noted, however, that other values of X/R would not influence the minimum and maximum limits of N shown in Figure 2 (i.e. Figure 4-10 of this report).

TABLE I

MINIMUM AND MAXIMUM POSSIBLE VALUES OF H FOR
EQUATION (6)

	$H\left(\dfrac{R}{L}, \omega\right)$	
	$\dfrac{R}{L} > 1.5$	$\dfrac{R}{L} \ll 1$
3-phase fault flat configuration		
center phase a	small	3.46
outside phase b	1.44	4.74
outside phase c	1.44	1.44
Phase-phase fault		
both phases	2.0	6.0

Note: $\omega_p/\omega > 5$.

Figure 4-9
Values for H from [4]
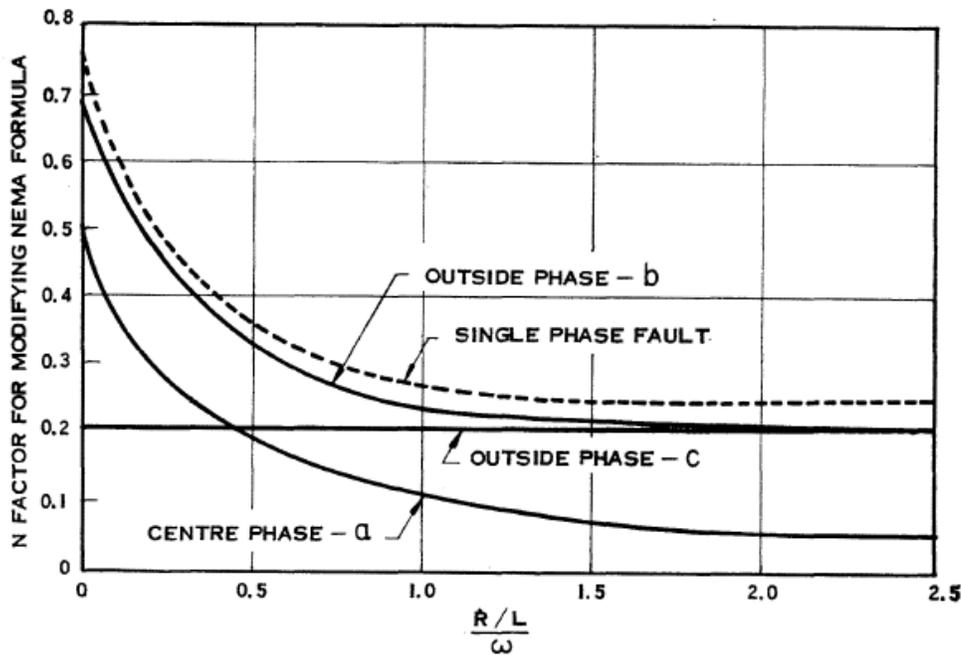
Figure 4-10
Attri-Edgar N Factor [4]

The Edgar Model

The Edgar model, as summarized by Barrett et. al. [7], relates cantilever forces to electromagnetic forces based on the simple mass-spring model as the Attri-Edgar Method. The distinction between the two approaches is the static SC force calculation and derivation of the dynamic factors. The single-phase without offset EM force is calculated with the following equation:

$$F_o = \frac{(\mu_0/2\pi)I_{SC}^2}{S}(L\alpha) \tag{3.14}$$

where

I_{SC} = the RMS symmetrical current, A

S = the perpendicular distance between conductors, m

L = the span length, m, and

α is the span factor.

The span factors are the same ones that would be used with the IEEE or IEC 865-1 methods. The cantilever force is then calculated using the following equation:

$$F_{cant} = F_o E_p \tag{3.15}$$

where

E_p = the Edgar factor with p = 1 for single-phase faults and p = 3 for three-phase faults as shown below in Figure 4-11.
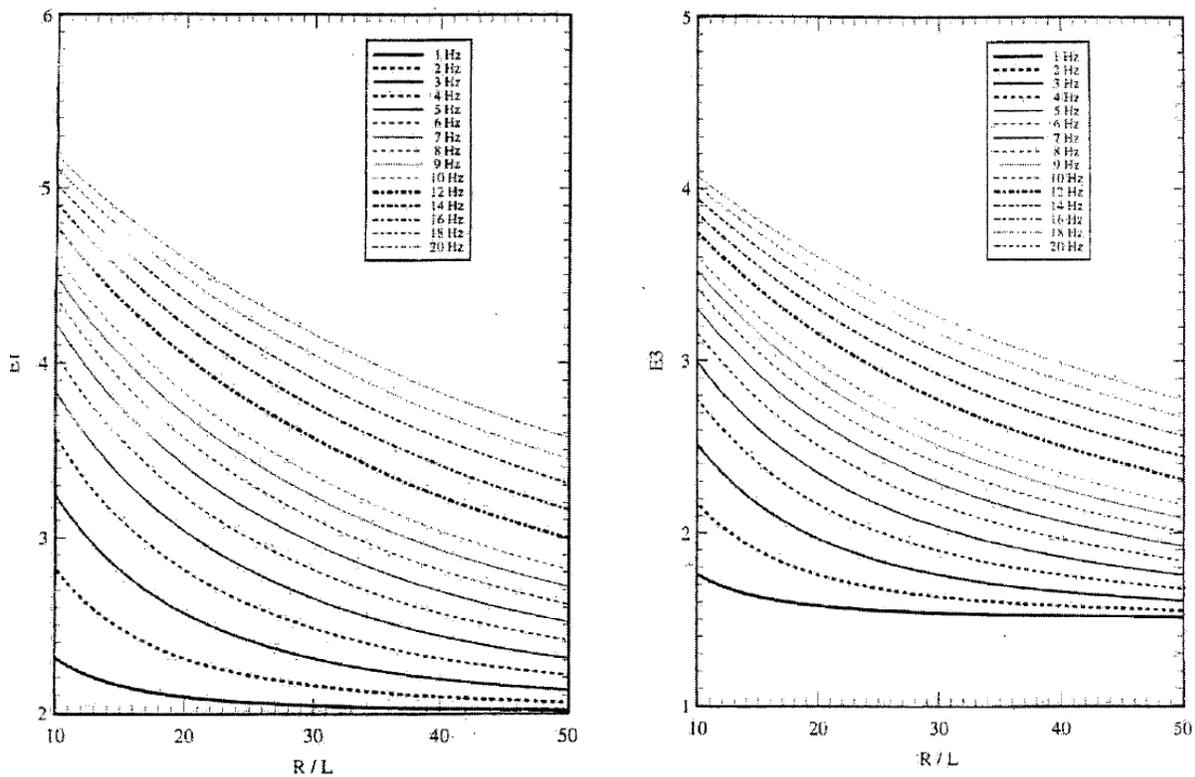
Figure 4-11
Line-to-line fault Edgar Factor (left) and Three-phase fault Edgar Factor (right) [7]

The Edgar factor takes into the account "the offset of the current waveforms and the decay of the offset". It requires knowledge of the bus natural frequency and the R/L as inputs. The authors do

not state this but it appears that the curves were derived using equations (3.9) and (3.12) and equating the spring force ky(t) to the product $H\left(\frac{R}{L}, \omega\right) F_o$ as done in equation (3.10) for the NEMA SC force calculation with one exception: Attri and Edgar appeared to smooth out the resonance points. This is illustrated and discussed in more detail in the Comparison of Dynamic Factor in section 5.

The authors of [7] provide a formula to relate the value of the spring constant of an insulator, which is specified for the top of the insulator, to the value of the spring constant at bus height in order to make a more accurate estimation of mechanical natural frequency.

$$K_1 F_{cant} = F_o E_p \frac{K_I}{r^3 - (1 - r)^3} \tag{3.16}$$

where

K_I = the insulator spring constant at the top of the insulator

r = the ratio a to b,

a = the difference between the bus height and the base flange height, [m] and

b = the difference between the insulator height and the base flange height, [m].

The authors state that there is a 20% and 50% reduction in the spring constant for 230 kV and for 46 kV insulators, respectively.

Dynamic Maximum Response Factor (DMF) Model

A simplified, generalized coordinate method for determining the frequency-based response of a rigid bus to SC forces was developed by Amundsen, Oster and Malten [5]. It involves calculating the static SC force between the conductors of a three-phase bus system using the equations presented in IEEE Std. 605-1998, and then reducing this maximum force value by a Dynamic Maximum Response Factor (DMF). The maximum SC induced stresses can then be computed and compared with values of conductor and insulator maximum yield stress to establish a maximum bus span length.

The DMF approach is based on the following common rigid-bus assumptions:

1. Assume only the first mode of vibration.
2. Conservatively assume no damping.
3. Assume rigid bus spans behave independently.
4. Assume insulators act as structurally fixed supports corresponding to rigid or slip bus support fittings.
5. Treat beams as a distributed mass system.

The steps involved in the DMF method are listed below. See [5] for details on each step.

1. Choose a shape function representing the deflected shape of the beam $\psi(x)$, such as the standard equation for the deflection of a fixed-fixed beam with the distributed load set equal to unity.

2. Calculate the first and second derivatives of the shape function.

3. Calculate the generalized mass of the beam from:

$$m_g = \frac{w}{g} \int_0^L [\psi(x)]^2 \, dx \qquad (3.17)$$

   where

   m_g = generalized distribution of mass along the beam, lb/in,

   w = weight per foot of the rigid bus span, lbf/in,

   g = gravitational constant = 386 in/sec^2,

   $\psi(x)$ = shape function previously defined,

   L = length of the beam, in

4. Calculate the generalized beam stiffness using:

$$k_G = EI \int_0^L [\psi''(x)]^2 \, dx \qquad (3.18)$$

   where

   k_G = generalized beam stiffness, lb/(in-sec^2),

   E = modulus of elasticity of the beam, psi,

   I = moment of inertia of the beam, in, and

   $\psi''(x)$ = second derivative of the shape function.

5. Calculate the natural circular frequency of the beam (rad/sec) with the following equation with the generalized mass and stiffness defined above:

$$\omega_n = \sqrt{\frac{k_G}{m_G}} \qquad (3.19)$$

6. Calculate the generalized short-circuit force for the shape function with:

$$F_G = F_{SC} \int_0^L \psi(x) dx \qquad (3.20)$$

   where

   F_G = generalized short-circuit force for the shape function, lbf/in, and

   F_{SC} = short-circuit force calculated using IEEE Std. 605, in lbf/in.

7. Noting that the deflection everywhere in the beam is at a maximum at the same time the deflection at midpoint is a maximum; use the general solution of the displacement at mid-span with the following equation:

$$v_m(t) = \left[\frac{F_G}{k_G} \frac{1}{1-\beta^2} (sin\, \omega t - \beta\, sin\, \omega_n\, t) \right] \psi_m \qquad (3.21)$$

where

$v_{m(t)}$ = general solution of deflection at midspan vs. time, in

F_G = generalized SC force for the shape function, lbf/in,

ω = circular frequency of the forcing function, rad/sec,

t = time (ranging from 0 to the fault clearing time, t_f), sec

β = ratio of the forcing frequency to the natural frequency (ω/ω_n)

k_G = generalized beam stiffness, lb/(in-sec²)

ψ_m = the deflection value of the shape function evaluated at mid-span, i.e.,
$\psi(x=L/2)$

8. Plot the general solution for mid-span deflection over the duration of the fault and locate the maximum mid-span deflection (Δ_{max}).

9. Calculate the static component of the maximum mid-span deflection using:

$$\Delta_{st\,st} = \frac{F_G}{k_G} \psi_m \qquad (3.22)$$

10. Calculate the dynamic maximum response of the rigid bus span to the forcing function from:

$$DMF = \frac{\Delta_{max}}{\Delta_{st}} \qquad (3.23)$$

11. Finally, compute the equivalent static SC force applied to the bus with:

$$F_{SC\_EQ} = F_{SC}\, DMF \qquad (3.24)$$

Design the rigid bus and insulators the usual way with the equivalent static SC force and an insulator overload factor of 2.0 or 2.5.

Amundsen, Oster and Malten apply their method to a hypothetical case study of a rigid bus configuration for a typical 138 kV substation in order to relate potential force reduction from the use of the DMF to expected cost savings.

The following design inputs define the case study:

1. The controlling stiffest span is a rigid-slip (i.e., structurally fixed-fixed) span with L = 26 feet or 312 inches.

2. The phase spacing is D= 8 feet or 96 inches.

3. The bus conductor is 5" Schedule 40 6061-T6 aluminum bus (E=10^7 psi, I = 20.7 in^4 and a self-weight of 8.26 lbf/ft= 0.6883 lbf/in including the damping wire)

4. The system electrical frequency is 60 Hz.

5. The X/R ratio is equal to 20 and the corresponding decrement factor is 1.27.

6. The fault clearing time is $t_f = 0.083$ sec.

7. For a short-circuit load case with extreme wind, assume V=90 mph controls.

8. Extreme wind load on the bus is $F_w = 9.4$ lbf/ft.

9. Insulator overload factors are:

10. K1 = 2.5 for wind load

11. K2 = 1.6 for short circuit load without dynamic reduction

12. K2 = 2.5 for short-circuit load with dynamic reduction

13. Decrement factor, $D_f = 1.27$

The results of this case study are summarized below:

Static short circuit force, $F_{sc} = 39.2$ lbf/ft

DMF = 0.23

$F_{sc\_EQ} = 9$ lbf/ft

Therefore, for this case study, accounting for bus dynamic response in the calculation of SC force reduced the predicted force level by 77%.

5
COMPARATIVE PERFORMANCE ASSESSMENT OF SC FORCE MODELS

Before concluding this work it is important to make a comparison of the various SC force models. First, the static SC force calculation of the methods will be compared. Then, the dynamic factors will be studied side-by-side. Finally, the accuracy of the methods will be investigated by comparing the calculation cantilever forces on the insulator-support with published empirical data of short circuit testing on rigid-bus assemblies. This comparative performance assessment considers the following SC force methods described in Section 4.

- IEC 865-1 Simplified Method [6]
- IEC 865-1 Detailed Method [6]
- DMF Method [**Error! Reference source not found.**]
- Attri-Edgar Method [4]
- IEEE Std. 605-2008 [3]
- IEEE Std. 605-1998 [2]
- Edgar Method [4]-[7]

Comparison of Static Short Circuit Force

The static SC force refers to the SC force calculated based on the asymmetric peak SC current (i.e. before the inclusion of a correction factor for the dynamic response). In the case of the Edgar Method, the calculation is based on the symmetrical SC current and therefore it represents the lower limit. Figure 5-1 shows the static SC force of all of the methods over a range of symmetrical SC current from 10 kA to 100 kA with the asymmetry and the conductor spacing of CIGRE Structure D [20]. The following observations are then made concerning the calculation methods:

1. The calculation of NEMA SG-6 [12], which is the static calculation used in the Attri-Edgar Method is by far the most conservative estimate of static short circuit force. This is not surprising considering since it is the oldest formulation.

2. The static calculation of IEC 865-1 [6] and IEEE Std. 605-2008 [3] are the same, although this might not be obvious at first. The reason is that [3] calculates the SC force with the maximum current asymmetry and then corrects the calculation to account for the actual asymmetry whereas [6] calculates the SC force with κ, which accounts for the asymmetry.

3. IEEE Std. 605-1998 [2] is much less conservative than the other three methods that use the asymmetric current.

4. The calculation of [2] is dependent on the duration of the short circuit with higher forces predicted for shorter SC durations. This contradicts the theoretical analysis presented in [13] where the maximum loading is predicted to occur when the short circuit duration is between ¼ and ½ of the period of the fundamental mechanical frequency. The discussion section of [13] also included in the discussion section a short review of experimental research at KEMA that confirmed the prediction of the authors.

5. There is a tendency towards increasing fault current levels as well as asymmetric (i.e. DC) time constants in power system networks [14]. Therefore, as the asymmetric fault currents increase, the conservatism of IEEE Std. 605 will become more and more significant (i.e. costly) with time.
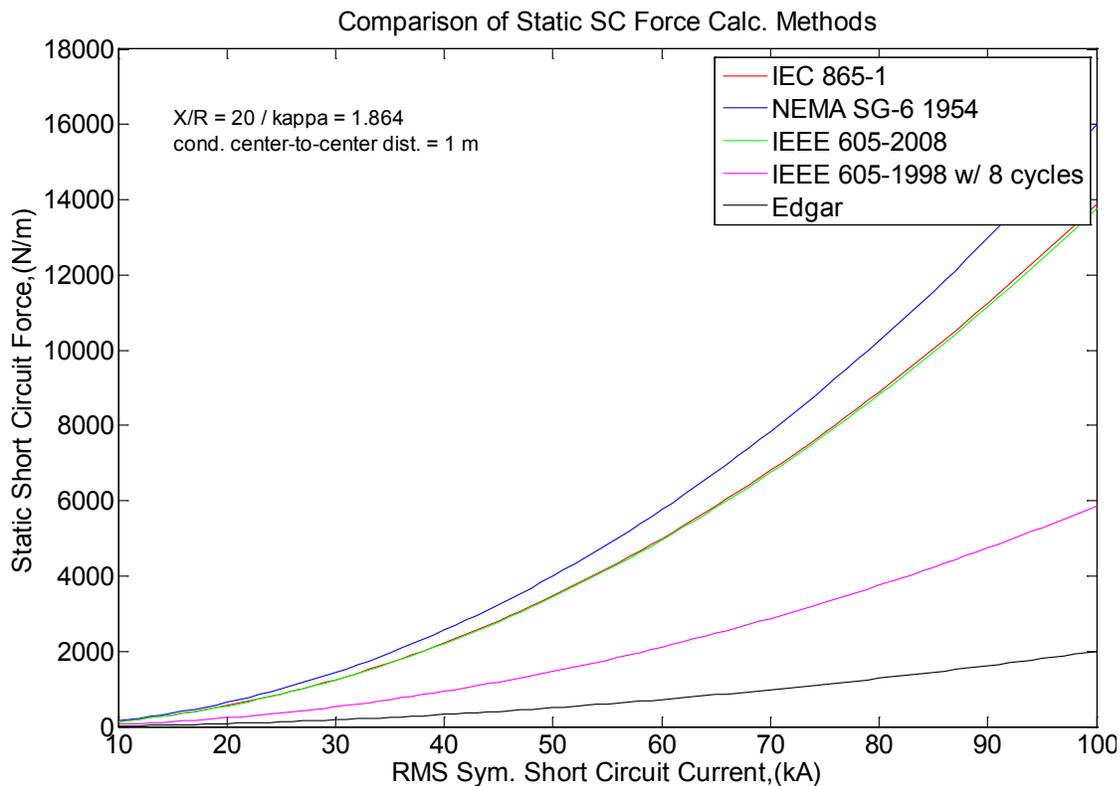
Figure 5-1
Comparison of Static SC Force of SC Force Calculation Methods

Comparison of Dynamic Factor

The dynamic factors of the IEC 865-1, DMF, Attri-Edgar and the Edgar Methods are plotted in Figure 5-2 and Figure 5-3 as a function of ratio of the bus assembly natural frequency to the power system frequency using the properties of the CIGRE Structure D. Figure 5-3 shows a close-up view of the dynamic factors of IEC 865-1 and Attri-Edgar. The following observations are made about the plots:

1. The DMF and Edgar Methods show a resonant response of the bus assembly with the forcing of the fundamental power system frequency (i.e. 50 Hz for CIGRE Structure D).

2. The Edgar Method also shows the resonant response to the double power system frequency.

3. The IEC 865-1 Method appears to clip off and moderately smooth the resonant peaks at the electrical fundamental and double frequencies.

4. The Attri-Edgar Method appears to completely smooth out the resonant peak.

5. The DMF appears to have a theoretical value of zero as the frequency ratio approaches zero whereas the factors of IEC 865-1 and Attri-Edgar Methods are closer to 0.3.

Comparison of Dynamic Factors for CIGRE Structure D
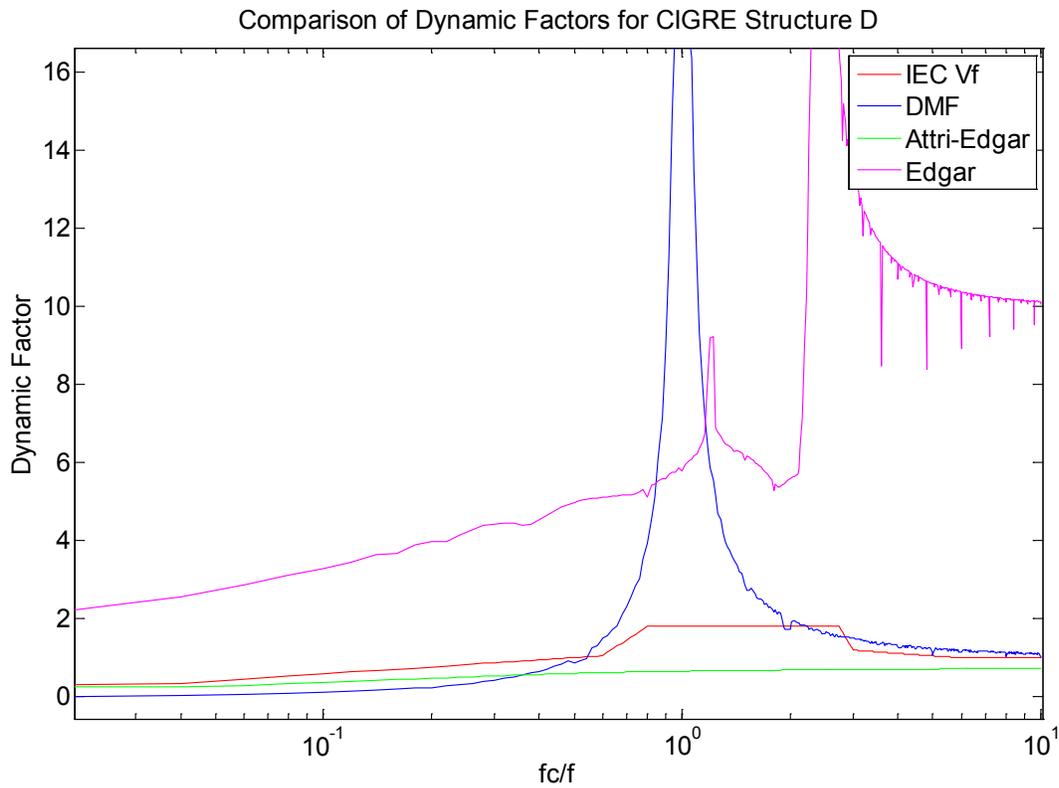
Figure 5-2
Comparison of Dynamic Factors of SC Force Calculation Methods
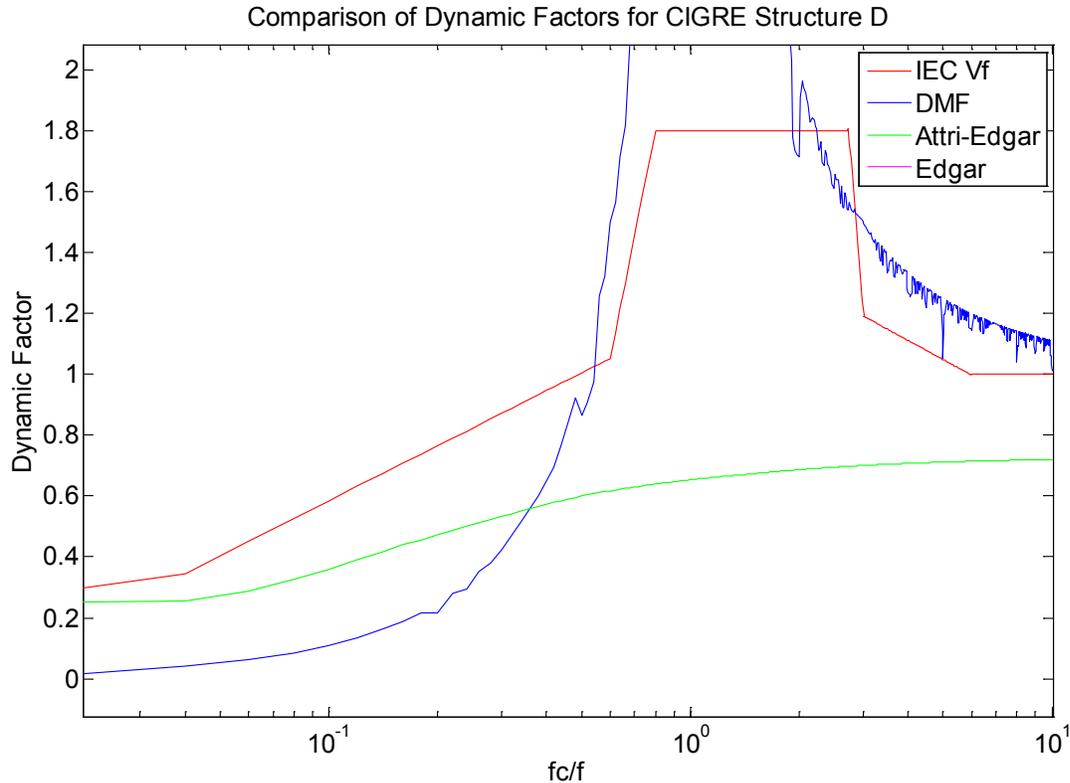
Figure 5-3
Up-close View of Figure 5-2

Accuracy Assessment of Methods

There are three subjects to be covered in the accuracy assessment of the SC force methods: the empirical data, an assessment of the accuracy of the natural frequency calculations of the methods with dynamic factors and the short circuit force accuracy assessment.

Empirical Data

The experimental results as presented in [7], [15]-[22] were reviewed and catalogued. The examples provided in [23] have complete datasets for SC force calculations. However, they are not included from the start since there is no mention or reference to real short circuit testing and corresponding measurements. The overall dataset is comprised of twenty-seven short circuit tests with three reclosures from thirteen different test sites. Some sites had multiple bus assembly arrangements. The datasets were then evaluated for appropriateness for a comparative study based on three requirements:

1. Ideal busbar arrangements (i.e. flat parallel busbar)

2. Minimum conductor spacing in order to neglect proximity effects

3. Measurement of force or stress on support insulators provided in publication

The datasets that did not meet all of the requirements were eliminated from the catalogue of data. Datasets that did not meet the first requirement include case 2 of [17], which has tests of parallel busbar with an inclined span (i.e. either 45 ° or 90 °) and [15], which is of a patented design of

two spans with a hopover. The simplified models considered in this report are not suitable for force calculations in or around curved or angle bus. The author of [16] was investigating the dynamic response of busbar supports in the 1920s and his work as presented in [16] is seminal. However, the bus used in the testing is rectangular and the spacing is less than double of the largest dimension. It was decided that the ratio of the conductor center phase distance (i.e. spacing) to the conductor outer diameter (OD) or effective diameter should be no less than five times. Therefore the results of [16] were excluded. The set up of [18] also has a low ratio of spacing to OD (i.e. 5.5) but the data was included. There is a discussion of a laboratory (i.e. bench top) set up in [21] but the data is excluded since the authors did not provide any information on the insulator SC force.

The remaining datasets are made of fourteen tests plus three reclosures from nine different test sites. See Section 9 – Empirical data for the complete listing of the data. Table 5-1 summarizes the key parameters of the datasets. For all but one of the datasets, the bus assembly parameters (not including the conductor spacing) represent high voltage bus assemblies for substations with a wide range of rated voltage from 138 kV to 500 kV. In most cases, the researchers simulated the forces of a substation with large short circuit capacity (SCC) (i.e. 10,000 to about 30,000 MVA and perhaps more) by decreasing the conductor spacing. In all cases, the test set up was chosen to be single-phase instead of three-phase. The reason is that the waveform of the largest force (i.e. on one of the outer conductors) in the event of a three-phase fault is similar to the forces on the conductors in the event of the line-to-line fault. The maximum three-phase short circuit force can be then be measured in a single-phase set up with reduced spacing and then scaled up for the three-phase. Unfortunately, there does not seem to be a consensus on how to relate the line-to-line test short circuit forces to design values for three-phase short circuits. The authors of [18] use an assumed ratio of 1 to 0.866 between three-phase and line-to-line short circuits and equate short circuit forces to calculate the necessary spacing with a given test current. The authors of [7] indicate that CIGRE 105 [17], the guidebook to [6], states that single-phase RMS symmetric test currents are related to equivalent three-phase currents as follows:

$$I_1 = \sqrt{0.808}\, I_3 \tag{5.1}$$

I_1= single phase RMS symmetric test currents

I_3 = equivalent three-phase currents

The authors of [7] later state that the approach of [17] is wrong and that the proper way to relate test currents and forces is to equate forces using (3.14) and (3.15). This approach gives the following formula relating the single-phase test current to the equivalent three-phase current:

$$I_1 = \sqrt{\frac{S_1 E_3}{S_3 E_1}}\, I_3 \tag{5.2}$$

The research community acknowledges the importance of studying the effects of reclosing and therefore three of the test set ups were used to study its effects. These results can be leveraged to study the performance of the methods with and without autoreclosure.

Finally, it is important to state that most authors did not give any indication of uncertainty in their measurements. The author of [22] provided an uncertainty of +/- 10% in the measurements

that he summarized. In the absence of any other information, this should serve as the best case uncertainty in the measurements used in this study.

Table 5-1
Key Parameters to Selected Datasets

Parameter Description	Min. Value	Mean. Value	Max. Value
Symmetrical RMS short circuit current, (kA)	7.5	31.9	64.3
Short circuit duration, (ms)	78	280	1030
Ratio of system reactance to resistance (X/R)	1.0	11.82	29.85
phase center to phase center distance, (m)	0.56	2.18	7.50
Span length, (m)	6.1	10.34	22.0
Number of spans	1	3	6
Bus conductor 2nd moment of area, (10^{-6} m^4)	0.032	11.66	24.86
Bus conductor weight per unit length, (N/m)	45.4	96.0	165.8
Measured bus assembly mechanical frequency, (Hz)	0.96	5.77	58.9

Accuracy Assessment of Natural Frequency Calculation Methods

Before comparing the results of the calculated insulator cantilever forces, the dynamic methods' calculations of bus assembly natural frequency should be considered. Table 5-2 shows a summary of the deviation of the calculated natural frequencies from the measured experimental values where an absolute deviation from the empirical value is calculated as shown below:

$$absolute\ deviation = \frac{absolute\ (f_{m,empirical} - f_{m,calculated})}{f_{m,empirical}}$$

The mean of the absolute deviations is calculated and is presented in Table 5-2. A detailed summary with plots are also given in Section 8 – Details of Comparative Assessment. Note that the concentrated masses at the supports have to be calculated to use the natural frequency calculation of the Attri-Edgar Method. In most cases, the weight of the insulator is not known and a reasonable value has to be assumed. The insulator spring constant is also not given in most instances. Therefore, the value is calculated with measured cantilever force and deflection of the insulator. The mass of the bus conductor is concentrated using the IEC 865-1 support factors.

Table 5-2
Mean Absolute Percent Deviation of Calculated Bus Assembly Natural Frequency with Measured Values

	IEC 865-1	IEEE Std. 605	DMF	Attri-Edgar
Mean Abs. Deviation	234%	109%	157%	120%

The following observations are made about the results:

1. No method's calculation is accurate in every case, which is why the mean value of all methods is so large. Refer to Section 8 – Details of Comparative Assessment to see the minimum and maximum deviation values for the methods.

2. The IEEE Std. 605's Method's calculation performs the best on average.

3. All methods' calculations, except the Edgar Method, are in gross error if the span length is small when the conductor size is typical of high voltage busbar (i.e. OD > 100 mm). This is true in the datasets for cases 5 and 6.

Accuracy Assessment of SC Conductor Bending Stress Calculation Methods

Table 8-2 shows a comparison of the calculated conductor bending stress of the methods in the case of an initial fault. For each method and for each test case, an absolute deviation from the empirical value is calculated in the same way as for the natural frequency calculations. The mean of the absolute deviations is calculated and is presented in Table 8-2. Similarly, Table 8-3 shows a comparison of the calculated conductor bending stress of the applicable methods in the event of a reclosure. Note that equation (1.13) from [2] is used to calculate the conductor bending stress given the span length, the short circuit force per unit length and conductor section modulus. Equation (1.13) is borrowed in order to make an estimate of conductor stress using the short circuit force predictions of the Attri-Edgar and Edgar Methods. The following observations are made about the results:

1. The predictions of IEEE Std. 605-1998 are the most accurate for an initial fault.

2. The predictions of IEC 865-1 are the closest for the one recorded reclosure event. However, the predictions of IEC 865-1 and IEEE Std. 605-1998 under-predict the measured values.

3. Attri-Edgar consistently over-predicts in both cases and might be used with an adjustment factor.

Table 5-3
Mean Absolute Percent Deviation of Calculated SC Conductor Bending Stress with Measured Values during Initial Fault

IEC 865-1 Simplified.	IEC 865-1 Detailed	Attri-Edgar	IEEE Std. 605-1998	Edgar
147.3%	20.7%	88.6%	14.3%	96.4%

Table 5-4
Mean Absolute Percent Deviation of Calculated SC Conductor Bending Stress with Measured Values during Reclosure

IEC 865-1 Simplified	IEC 865-1 Detailed	Attri-Edgar	IEEE Std. 605-1998	Edgar
67.7%	27.9%	35.9%	55.5%	44.7

Accuracy Assessment of SC Force Calculation Methods

Table 8-4 shows a comparison of the calculated inner and outer insulator cantilever forces of the methods in the case of an initial fault. The span factors as defined by IEC 865-1 are used for all of the methods. For each method and for each test case, an absolute deviation from the empirical value is calculated in the same way as for the natural frequency calculations. The mean of the absolute deviations is calculated and is presented in Table 8-4. Similarly, Table 8-5 shows a comparison of the calculated inner and outer insulator cantilever forces of the applicable methods in the event of a reclosure. The DMF are not included in this comparison since the method as documented by as documented by [5] do not have a factor that considers the effects of reclosing. The Attri-Edgar and Edgar methods as described in [4] and [7] also do not have a factor for reclosure. However, a constant (i.e. frequency independent) reclosure factor of 2.0 was employed. The reason is that the Ontario Hydro Method (i.e. Attri-Edgar Method) for the comparative study of [20] (see
Section 10 – Comparative Study of Advanced SC Force Prediction Methods) used a factor of 2.0 for calculating short circuit forces in the event of an autoreclosure.

Table 5-5
Mean Absolute Percent Deviation of Calculated Insulator Cantilever Forces with Measured Values during Initial Fault

	IEC 865-1 Simplified.	IEC 865-1 Detailed	DMF	Attri-Edgar	IEEE Std. 605-2008	IEEE Std. 605-1998	Edgar
Outer Support	118.7%	7.3%	95.2%	10.9%	80.4%	11.1%	6.8%
Inner Support	408.4%	143.6%	74.2%	66.5%	232.7%	71.8%	87.5%
Overall	325.6%	104.7%	80.2%	50.6%	189.2%	54.5%	64.4%

Table 5-6
Mean Absolute Percent Deviation of Calculated Insulator Cantilever Forces with Measured Values during Reclosure

	IEC 865-1 Simplified	IEC 865-1 Detailed	Attri-Edgar	IEEE Std. 605-2008	IEEE Std. 605-1998	Edgar
Outer Support	3.4%	15.9%	2.8%	4.1%	66.3%	9.5%
Inner Support	285.0%	147.2%	86.5%	98.6%	24.5%	125.1%
Overall	238.1%	125.3	72.5%	82.9%	31.5%	105.8%

The following observations can be made from the results of Table 8-4 and Table 8-5 for the parameter space covered in this comparative assessment.

Observations for Study of Short Circuit Force Predictions without Reclosure

1. As expected, the calculated SC insulator cantilever forces predicted by IEEE Std. 605-2008 are overly conservative with respect to actual, measured values for the case of an initial short circuit (i.e. short circuit without reclosure). The absolute average deviations for the outer and inner supports are 83.4% and 232.7, respectively.

2. The method with the most conservative predictions for the case of an initial short circuit (i.e. short circuit without reclosure) is the IEC 865-1 simplified method. The absolute average deviations for the outer and inner supports are 118.7% and 408.4, respectively.

3. The method with the best predictions for the inner support cantilever force for the case of an initial short circuit (i.e. without reclosure) is the Attri-Edgar Method. The average absolute deviation from the measured values is 66.5%.

4. The method with the best predictions for the outer support cantilever force for the case of an initial short circuit (i.e. without reclosure) is the Edgar Method. The average absolute deviation from the measured values is 6.8%

5. The method with best overall predictions for support cantilever force for the case of an initial short circuit (i.e. without reclosure) is the Attri-Edgar Method. The weighted average absolute deviation from the measured insulator cantilever force is 52.6%. The calculation of IEEE Std. 605-1998 was slightly worse at 56.6%.

6. All methods perform significantly better at predicting the outer support cantilever force with respect to inner support cantilever force. The error is as much as 20 times more for the IEC 865-1 Detailed Method and as little as 3 times for IEEE Std. 605-2008. The one apparent exception to the observation that the outer support force prediction is better than the inner support force prediction is the DMF Method. However, the results of the DMF method for the outer support calculations are only slightly better than for the inner support calculations. Also the reason is also partly attributable to the fact that the frequency calculation of the DMF is much too large for several cases, which leads to an artificially high DMF (i.e. dynamic factor).

Observations for Study of Short Circuit Force Predictions with Reclosure

The forces during a reclosure are most accurately predicted by IEEE Std. 605-1998. The overall average absolute deviation from the measured values is 31.5%. However, the forces are sometimes well below the measured values. The predictions of the Attri-Edgar Method have more error with an overall deviation of 72.5% but they consistently over-predicted, which makes this method more useful in practical bus design.

6
CONCLUSIONS AND RECOMMENDATIONS

Based on the research and analyses performed in this study, and described in this report, the following conclusions are drawn:

1. The methodology provided in IEEE Std. 605 for calculating SC forces on rigid, sub-station bus work is viable for use at increased fault current levels, although it yields conservative results. Manual calculations of SC force for a realistic busbar configuration matched reasonably close to the EM FEA model predictions.

2. It is possible to increase accuracy in the IEEE Std. 605 methodology for predicting SC force and corresponding mechanical stresses experienced by the bus structure by accounting for the dynamic response of the bus system to the fault current forcing function. This is seen in Table 5-5 where the predictions by the Attri-Edgar and the IEC 865-1 methods are significantly closer to the measured values than the IEEE Std. 605 results.

3. In the calculation of bus assembly natural frequency, no method seems to always calculate the correct natural frequency. However, the Attri-Edgar method is the only the method that includes the contribution from the elasticity of the insulators and the bus. Therefore it is expected to be more accurate than the more simplified methods with the proper parametric data.

4. In the prediction of conductor bending stress, the method of IEEE Std. 605-1998 provided the most accurate results. However, the calculation of Attri-Edgar over-predicted consistently and might be the preferable approach with a correction factor.

5. In the prediction of short circuit insulator cantilever force without reclosure, the Attri-Edgar Method produced the closest values to the measured values.

6. In the prediction of short circuit insulator cantilever force with reclosure, the Attri-Edgar Method produced the closest values to the measured values that do not drastically underestimate the forces.

Based on these conclusions from this limited study, it is recommended that:

7. The calculation of bus assembly natural frequency should be computed with the Attri-Edgar Method if the insulator spring constants are available. If the spring constants are not known, then the method of IEEE Std. 605-1998 should be used.

8. The calculation of insulator cantilever forces (and also bus conductor bending stress if a proper correction factor can be found) should be computed with the Attri-Edgar Method. Because of this recommendation, the code for the Attri-Edgar Method written in MATLAB is provided in Section 11 – Computer code for Attri-Edgar Method.

9. A similar study shall be performed for flexible (i.e., strain) bus systems

7
REFERENCES

1. "Fault Current Management Guidebook – Update", EPRI, Palo Alto, CA, 1012419, 2006.

2. IEEE 1998, Standard 605, "IEEE Guide for Design of Substation Rigid-Bus Structures", New York, NY.

3. IEEE 2008, Standard 605, "IEEE Guide for Bus Design In Air Insulated Substations", New York, NY.

4. N.S. Attri, and J.N. Edgar, "Response of Bus Bars on Elastic Supports Subjected to a Suddenly Applied Force", IEEE Transactions on Power Apparatus and Systems, Vol., PAS-86, No. 5, May 1967.

5. Amundsen, T.A. J.L. Oster, and K.C. Malten, "Analytical Techniques to Reduce Magnetic Forces from High Fault Current on Rigid Bus", presented at the Electrical Transmission and Substation Conference, ASCE, 2009.

6. IEC 1993. "International Standard 865-1: 1993. Short circuit Currents—Calculation of Effects. Part 1: Definitions and Calculation Methods". Genève: CEI.

7. Barrett, J.S., W.A. Chisholm, J. Kuffel, C.J. Pon, B.P. Ng, A-M. Sahazizian, C. de Tourreil, "Testing and Modelling Hollow-Core Composite Station Post Insulators Under Short-Circuit Conditions", PES General Meeting, 2003.

8. Notes-Teleconference with Southern Company, EPRI, and FSU-CAPS, August 29, 2011.

9. IEEE 206, Standard C57.12.00, "IEEE Standard for Standard General Requirements for Liquid-Immersed Distribution, Power and Regulating Transformers", New York, NY.

10. F. T. Ulaby, Fundamentals of Applied Electromagnetics, Pearson Education, 2004.

11. Companion Book for CIGRE Brochure 105. "The Mechanical Effects of Short-Circuit Currents in Open Air Substations (Part II)".

12. Power Switching Equipment. NEMA Standards Publication No. SG6, National Electrical Manufacturers Association, New York, N.Y., Oct. 1954.

13. D.K. Tsanakas, B.C. Papadias, "Influence of Short-circuit Duration on Dynamic Stresses in Substations," IEEE Trans. on Power Apparatus and Systems, Vol. PAS-102, No. 2, February 1983.

14. R. P. P. Smeets, "The Impact of Increasing Fault Current on T&D Equipment," Conference on Electric Power Supply Industry, Oct. 2012.

15. W. Stefanik, Jr., G.A. Votta, J.M. Stipcevich, "Short Circuit Tests on a 3-phase, 230kV Rigid Bus Assembly," IEEE Trans. on Power Apparatus and Systems, Vol. PAS-98, No. 3 May/June 1979.

16. O.R. Schurig, M.F. Sayre, "Mechanical Stresses in Busbar Supports during Short Circuits", presented at Midwinter Convention of AIEE, Feb. 9-12, 1925.

17. CIGRE 105. "The Mechanical Effects of Short-Circuit Currents in Open Air Substations (Rigid and Flexible Bus-Bars)".

18. D. W. Taylor, C.M. Stuehler, "Short-circuit Tests on 138-Kv Busses," Trans. AIEE (Power Apparatus and Systems), Vol. 75, pp. 739-747, August 1956.

19. R. M. Milton and F. Chambers, "Behavior of High-voltage Busses and Insulators During Short Circuits," Trans. AIEE (Power Apparatus and Systems), Vol. 74, pp. 742-749, August 1955.

20. Hosemann, G. and Tsanakas, D., "Calculated and Measured Values of Dynamic Short-circuit Stress in a High Voltage Test Structure with and without Reclosure." Electra, No. 63, March 1979.

21. M. Iordanescu, C. Hardy, J. Nourry, "Structural Analysis and Testing of HV Busbar Assemblies with Rigid Conductors under Short-circuit Conditions," IEEE Trans. on Power Delivery, Vol. PWRD-2, No. 4, October 1987.G. Palante, "Behavior of Rigid Conductors and Their Supports under Short-circuit Conditions – Comparison of Calculated and Measured Values", CIGRE 1976, Report 23-10.

22. G. Palante, "Behavior of Rigid Conductors and Their Supports under Short-circuit Conditions – Comparison of Calculated and Measured Values", CIGRE 1976, Report 23-10.

23. IEC 1994. "International Standard 865-2: 1994. Short circuit Currents—Calculation of Effects. Part 2: Examples of Calculation". Genève: CEI.

24. O. Deter, R.R. Gibbon, G. Hosemann, N. Stein, "Measurement of Short-circuit Stresses on Rigid Conductor Busbar Systems and Comparison of Test Results," Electra No. 30, October 1973, pp. 35-54.

25. ABB Switchgear Manual, 10th Edition, 2001.

8

DETAILS OF COMPARATIVE ASSESSMENT

A more detailed look at the comparison of the calculated natural frequencies and short circuit insulator force are provided below. Note that for the comparisons of natural frequency and short circuit force, each short circuit test is assigned a unique number in hexadecimal that is consistently used in all of the figures. A short circuit followed by an autoreclosure is considered only one test and therefore both have the same number.

Section 9- Empirical data indicates which numbers apply to which test site and test data. In all figures, the experimentally measured values are plotted on the x-axis and the calculated values on the y-axis on a scatter plot. The line y = x (dashed line), on which data points for best predictions would fall, is also plotted for reference.

Details of Comparative Assessment of Natural Frequency Calculation Methods

A more detailed look at the comparison of the calculated natural frequencies is shown below in Figure 8-1 and Figure 8-2 and Table 8-1.
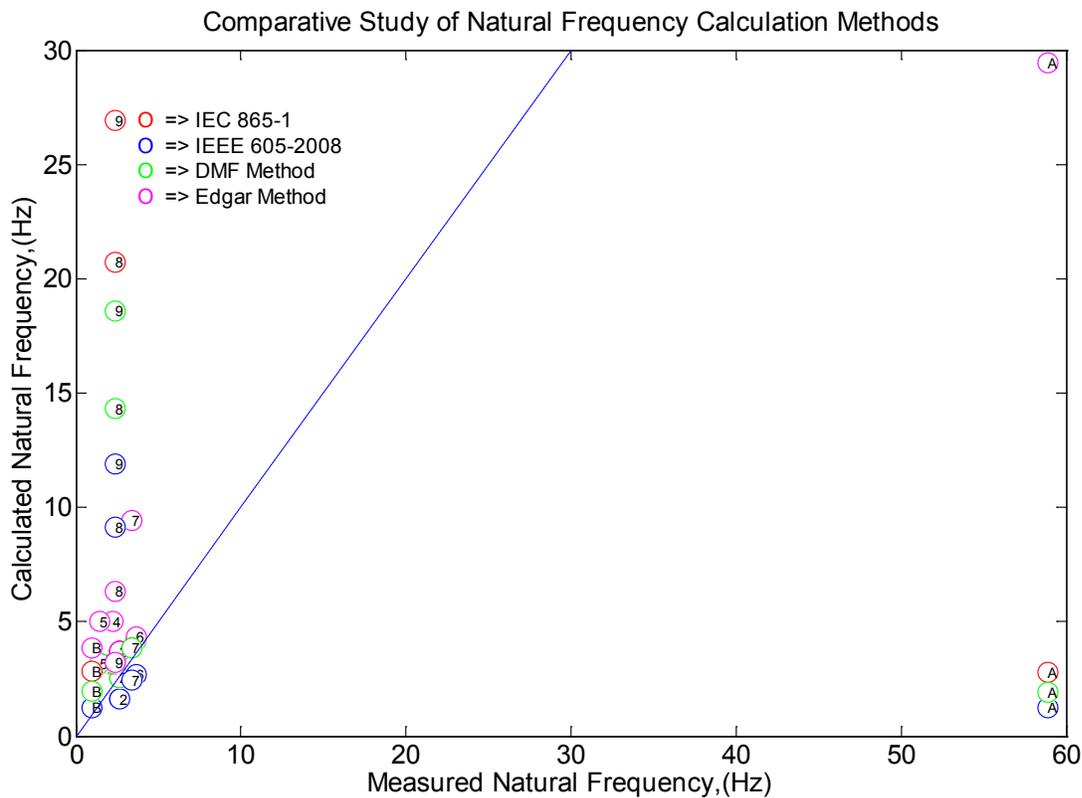
Figure 8-1
Comparison of Natural Frequency Calculation of SC Force Calculation Methods with Measured Natural Frequency
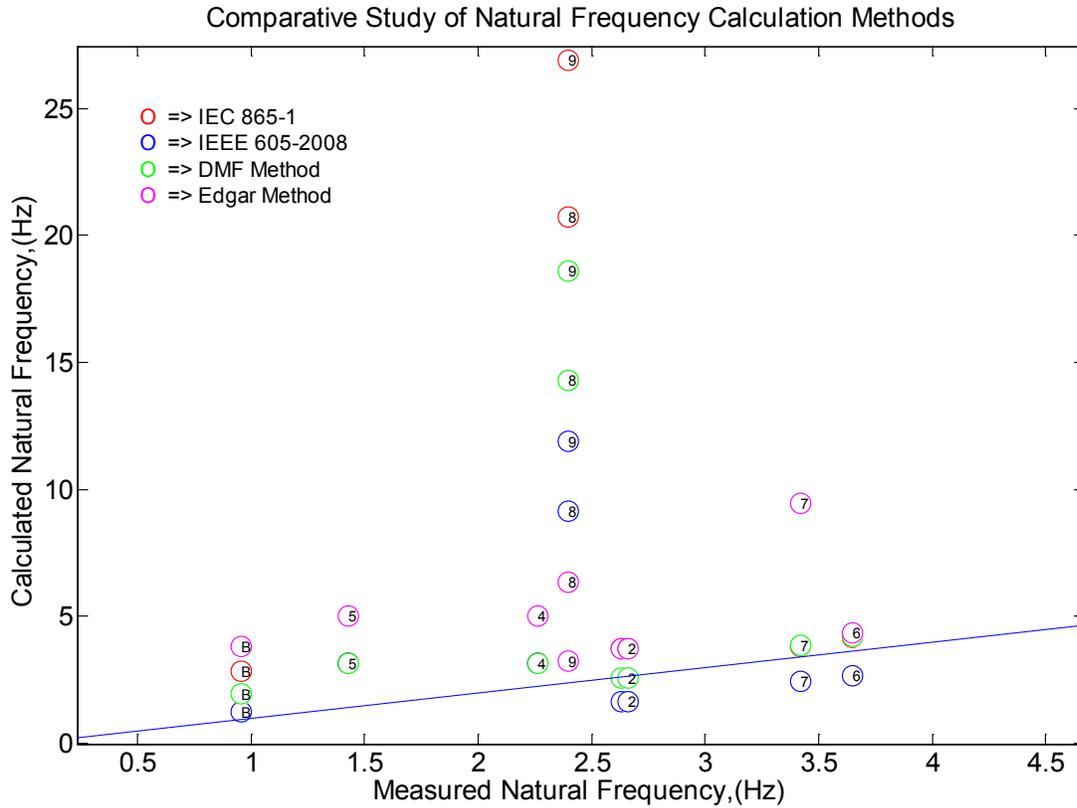
Figure 8-2
Up-close View of Figure 8-1

Table 8-1
Summary of Absolute Percent Deviation of Natural Frequency Calculations with Measured Natural Frequency

Method Name	Min	Mean	Max
IEC 865-1 Method	12.2	234.2	1021.5
IEEE Std. 605 Method	26.6	109.5	394.8
DMF Method	2.4	156.6	674.6
Attri-Edgar Method	19.4	119.6	299.3

Details of Comparative Assessment of Conductor Bending Stress Calculation Methods

A more detailed look at the comparison of the calculated conductor bending stress is shown below in Figure 8-3 and Figure 8-4 and Table 8-2 and Table 8-3.
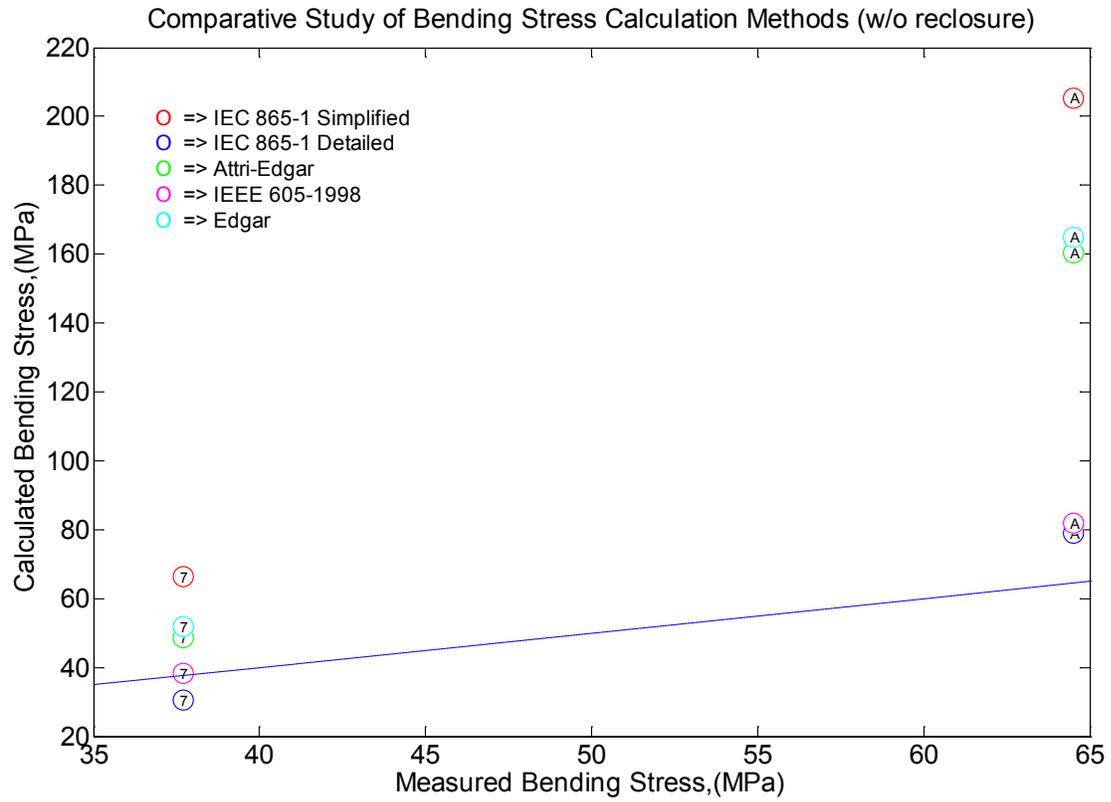
Figure 8-3
Comparison of Calculated Conductor Bending Stress without Reclosure
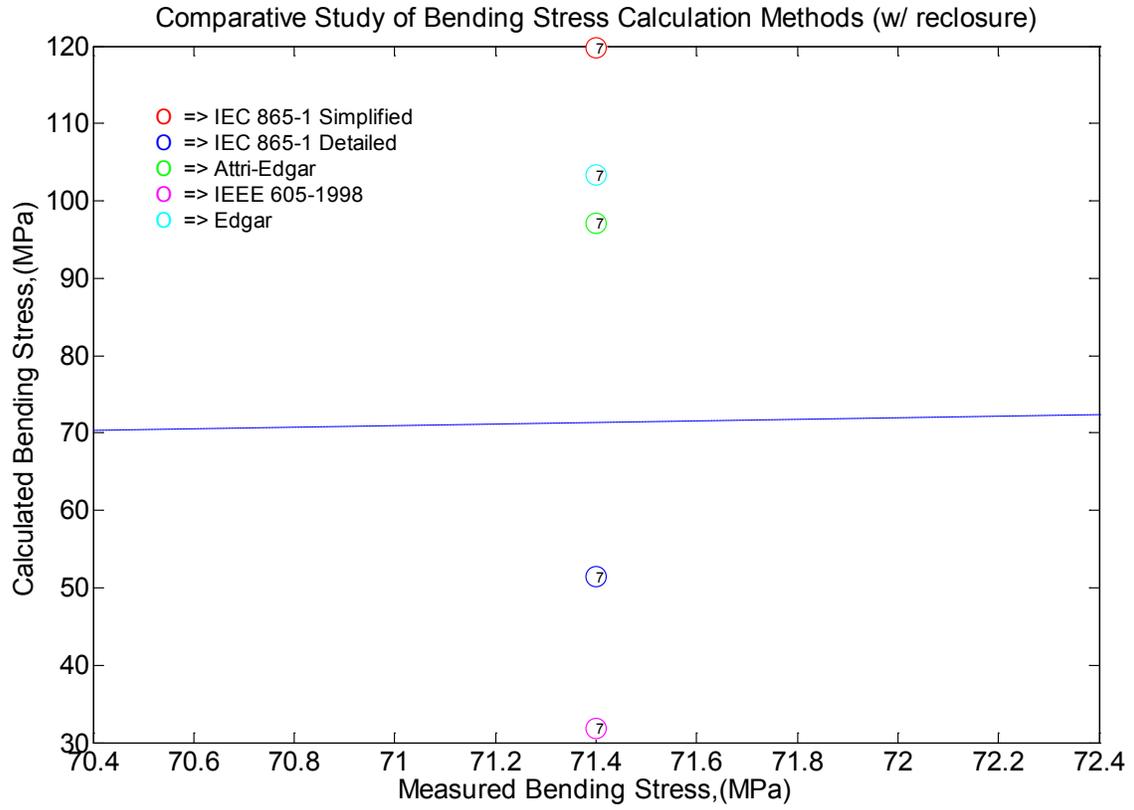
Figure 8-4
Comparison of Calculated Conductor Bending Stress with Reclosure

Table 8-2
Summary of Absolute Percent Deviation of Calculated Conductor Bending Stress without Reclosure

Method Name	Min	Mean	Max
IEC 865-1 Simplified Method	76.4	147.3	218.3
IEC 865-1 Detailed Method	19.0	20.7	22.5
Attri-Edgar Method	28.7	88.6	148.6
IEEE Std. 605-1998 Method	1.9	14.3	26.7
Edgar Method	37.0	96.4	155.8

Table 8-3
**Summary of Absolute Percent Deviation of Calculated Conductor Bending Stress with Reclosure**

Method Name	Min	Mean	Max
IEC 865-1 Simplified Method	67.7	-	-
IEC 865-1 Detailed Method	27.9	-	-
Attri-Edgar Method	35.9		
IEEE Std. 605-1998 Method	55.5	-	-
Edgar Method	44.7		

Details of Comparative Assessment of SC Force Calculation Methods

A more detailed look at the comparison of the insulator cantilever forces is shown below in Figure 8-5 through Figure 8-9. Figure 8-5 through Figure 8-7 show the inner and outer insulator cantilever forces on initial short circuit (i.e. without reclosure). Figure 8-8 and Figure 8-9 show the inner and outer support forces in the case of a reclosure. As mentioned previously, each short circuit test is assigned a unique number in hexadecimal that is consistently used in all of the figures. Also, if there is more than one measurement point from a test utilized in the comparison, then a different marker shape is used with the same number. The results of the DMF are not given in Figure 8-8 and Figure 8-9 since this method as documented by [5] does not have an adjustment to its dynamic factor to account for reclosure.
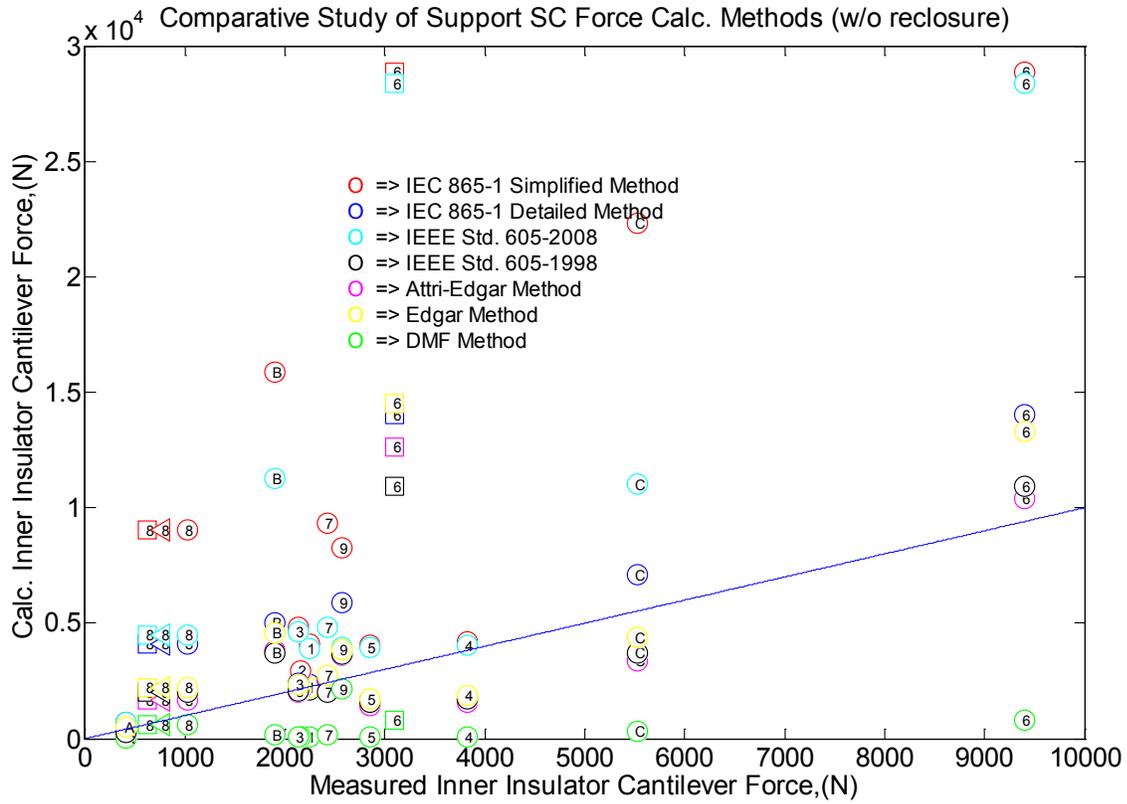
Figure 8-5
Comparison of Force Calculation Methods and Measured Data for Inner Insulator Cantilever Forces without Reclosure
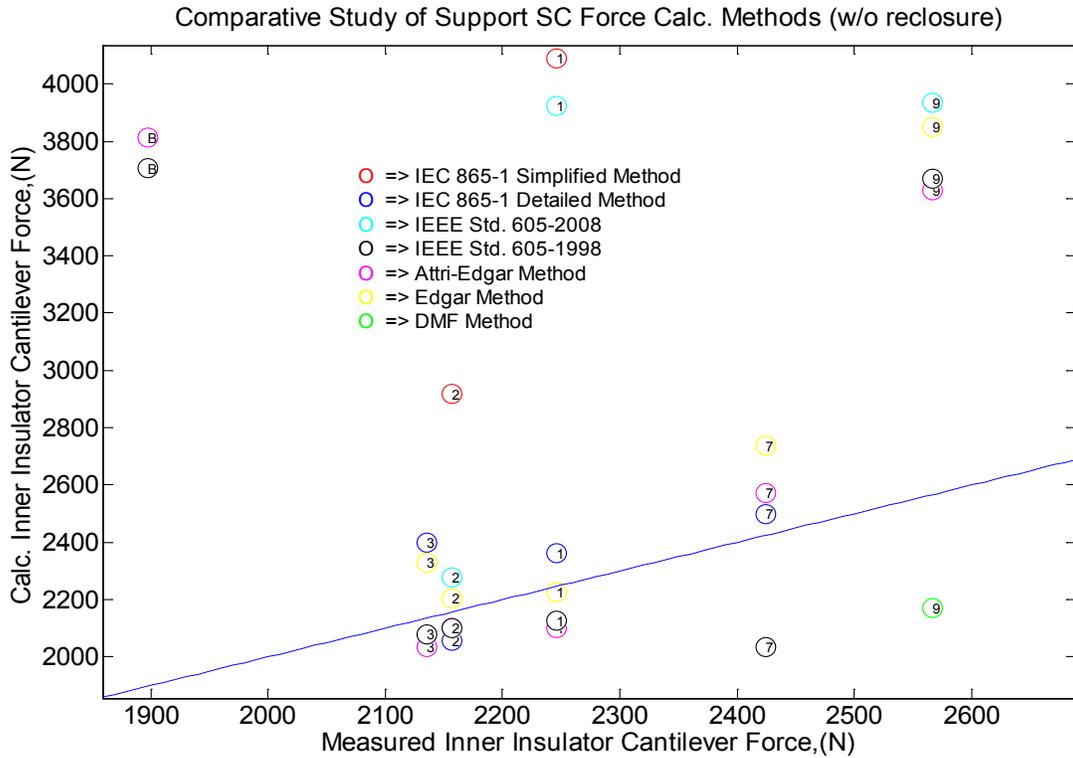
Figure 8-6
Up-close View of Figure 8-5
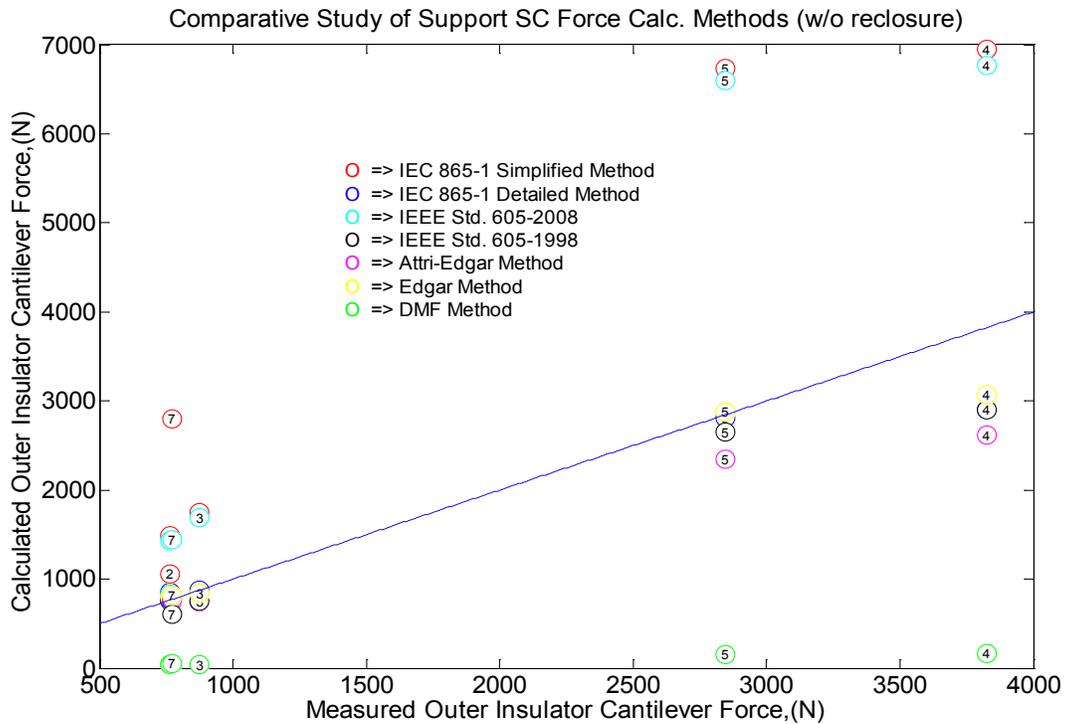
Figure 8-7
Comparison of Force Calculation Methods and Measured Data for Outer Insulator Cantilever Forces without Reclosure
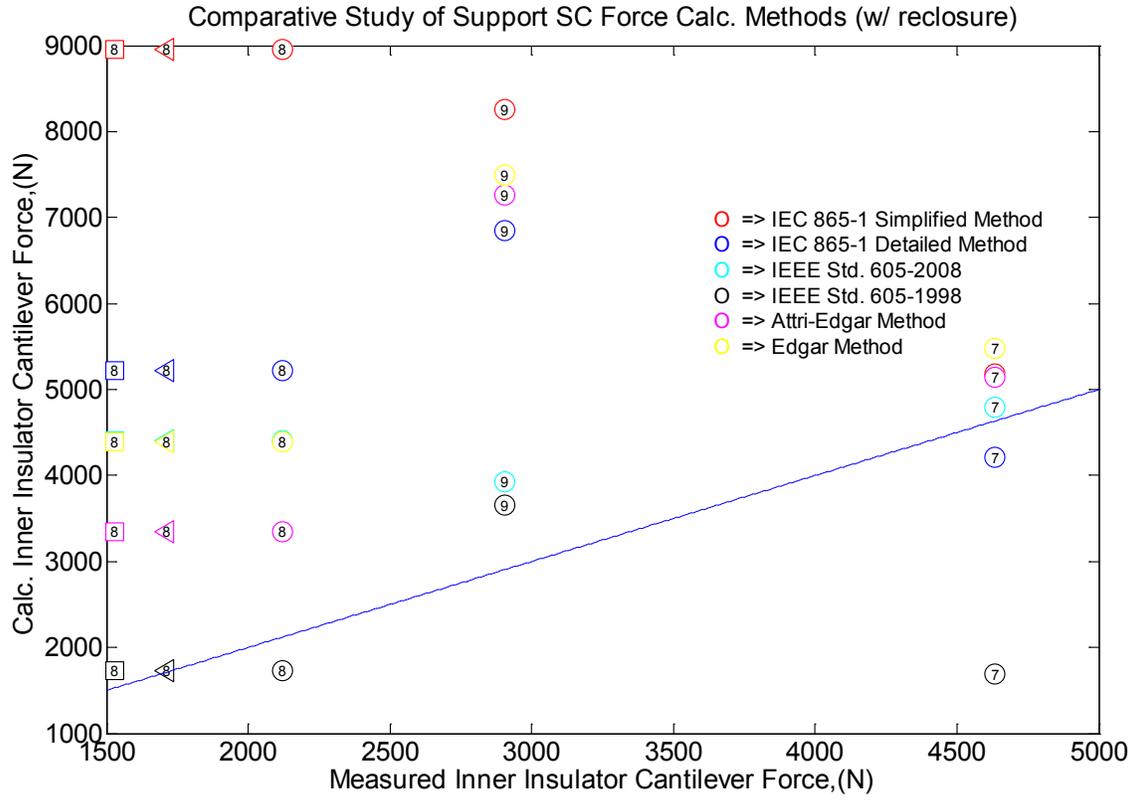
Figure 8-8
Comparison of Force Calculation Methods and Measured Data for Inner Insulator Cantilever Forces with Reclosure

Figure 8-9
Comparison of Force Calculation Methods and Measured Data for Outer Support Forces with Reclosure

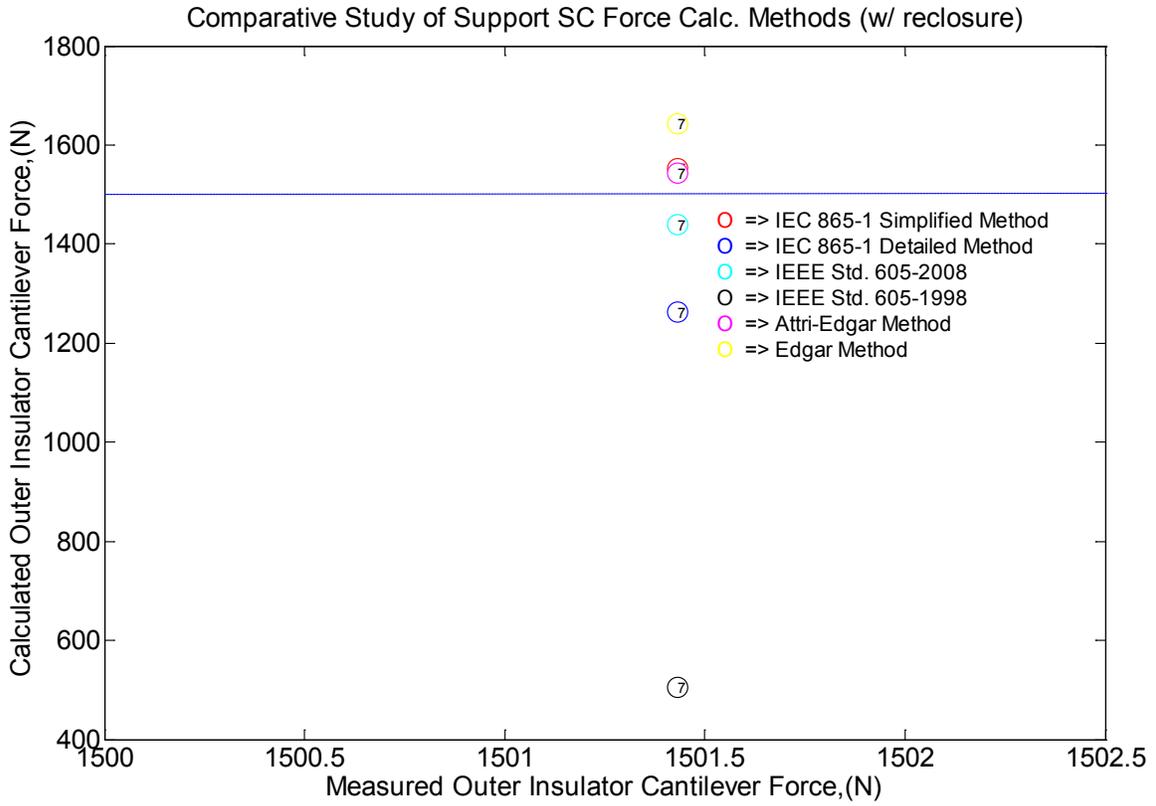The results are summed up with the minimum, mean and maximum absolute deviation of the calculated insulator cantilever force from the experimentally measured force in Table 8-4 and Table 8-5.

Table 8-4
Summary of Absolute Percent Deviation of Calculated Support Forces with Measured Values for Initial Short Circuit

Method Name	Inner support			Outer support		
	Min	Mean	Max	Min	Mean	Max
IEC 865-1 Simplified Method	9.0	408.4	1343.2	38.8	118.7	261.5
IEC 865-1 Detailed Method	3.0	143.6	555.2	4.6	7.3	24.3
DMF Method	6.6	74.2	97.6	93.6	95.2	96.0
Attri-Edgar Method	2.7	66.5	306.9	0.2	10.9	31.7
IEEE Std. 605-2008 Method	5.5	232.7	816.0	8.2	80.4	131.7
IEEE Std. 605-1998 Method	2.6	71.8	252.2	0.1	11.1	24.3
Edgar Method	1.0	87.5	367.5	1.1	6.8	19.6

Table 8-5
Summary of Absolute Percent Deviation of Calculated Support Forces with Measured Values During Reclosure

Method Name	Inner support			Outer support		
	Min	Mean	Max	Min	Mean	Max
IEC 865-1 Simplified Method	11.7	285.0	484.9	3.4	-	-
IEC 865-1 Detailed Method	9.2	147.2	240.9	15.9	-	-
Attri-Edgar Method	11.0	86.5	149.9	2.8	-	-
IEEE Std. 605-2008 Method	3.5	98.6	188.4	4.1	-	-
IEEE Std. 605-1998 Method	1.4	24.5	63.6	66.3	-	-
Edgar Method	18.2	125.1	186.7	9.5	-	-

9
EMPIRICAL DATA

There are nine different experimental set ups or cases utilized in the comparative assessment of the SC force calculation methods. Some cases have several SC tests or measuring points that have been included in the dataset as indicated by Table 9-1.

Table 9-1
Summary of Support Force/Stress Measurements

Case Number	Reference	Insulator/Steel Support Measurement Method	Inner Support Meas. Pts.		Outer Support Meas. Pts.		SC Tests Used	Recl.
			I	S	I	S		
1	[18]	1. Deflection measurement and static force measurement with dynamometer arrangement	1	0	0	0	3	N
2	[19]	1. Deflection measurement and static force measurement with dynamometer arrangement	N/A	N/A	1	0	2	N
3	[7]	1. Calculation using measured deflection and insulator spring constant 2. Strain gauge measurement	2	0	0	0	1	N
4	[20]	Bending moments provided. Measurement details given in [24]	1	1	2	2	1	Y
5	[17]	Not provided	3	0	0	0	1	Y
6	[21]	1. Strain gauge measurement (not converted to force)	1	1	0	0	1	Y
7	[22]	Not provided	1	0	0	0	1	N
8	[22]	Not provided	1	0	0	0	1	N
9	[22]	Not provided	1	0	0	0	1	N

The labels 'I' and 'S' refer to insulator and steel supports, respectively. The label 'Recl.' refers to autoreclosure. There are twelve short circuit tests utilized for the study, which is the sum of the column entitled 'SC Tests Used'.

Note that conductor moment of inertia and section modulus are frequently not provided, although the necessary geometric parameters are usually given. The minimum conductor stress yield point is also not usually given and a reasonable value has to be assumed. The insulator spring constant is also left most of the time. Therefore it is estimated using the published cantilever force and the insulator deflection. Sometimes the X/R ratio (i.e. the short circuit time constant) is not provided. In those instances, the X/R ratio is estimated using the ratio of asymmetric peak to the peak symmetric current. This number is known in the IEC standards as κ. [25] provides a formula to calculate κ given the X/R, which can be used to calculate X/R given κ:

$$\kappa = 1.02 + 0.98 e^{-\frac{3R}{X}} \tag{9.1}$$

Case 1 – Public Service Electric and Gas Company [18]

Twelve short circuit tests were conducted and the results of eight short circuit tests were published. The first six of those tests (tests #1 through #6) were done with an insulator stack with rated cantilever strength of 1700 lbs. The conductor was copper 3 ½" standard IPS tubing. The last six of the tests (tests #7 through #12) employed an insulator stack with rated cantilever strength of 1200 lbs. The conductor was copper tubing with 4" diameter with 1/8" wall thickness. The results of tests #5, #6 and #8 are used in this study. Note that the bus specific weight is calculated based on the geometric data provided and a value of 8900 kg/m³ for the density of the copper tubular conductor. The insulator spring constant is calculated based on the published cantilever force and the insulator deflection for test #5. When there is a difference in a parameter or test results between the tests, all values will be given as (test 5 value, test 6 value, test 8 value) or as (bus arrangement 1 value, bus arrangement 2 value).

Case 1 is represented by #1, #2 and #3 on all plots.

Figure 9-1
Test Structure for Case 1 [18]

Table 9-2
Case 1 Electrical Parameters

Parameter Description	Value
Short Circuit Current, (kA RMS)	(15.77, 15.77, 15.52)
Short Circuit Duration, (ms)	500
Ratio of system reactance to resistance, X/R	(3.16, 0.99, 4.73)
Electrical frequency, Hz	60
Line-to-line fault	Y
Reclosure	N

Table 9-3
Case 1 Conductor Parameters

Parameter Description	Value
Bus conductor outer diameter, (mm)	101.6
Bus conductor wall thickness, (mm)	(6.4, 3.2)
Bus conductor 2nd moment of area, (10^{-6} m^4)	(2.164, 1.19)
Bus conductor section modulus, (10^{-5} m^3)	(4.26, 2.34)
Bus conductor weight per unit length, (N/m)	(165.8, 85.7)
Bus conductor modulus of elasticity (GPa)	110.3

Table 9-4
Case 1 Bus Assembly Parameters

Parameter Description	Value
Phase center to phase center distance, (m)	0.56
Span length, (m)	10.67
Number of spans	3
Insulator spring constant, (N/mm)	135

Table 9-5
Case 1 Test Measurements

Measurement Description	Value
Max. inner insulator cantilever force, (N)	(2246, 2157, 2135)
Max. outer insulator cantilever force, (N)	(765, 765, 876)
Max. inner insulator deflection, (mm)	(16.59, 17.02, -)
Max. outer insulator deflection, (mm)	(5.44, 5.44, -)
Max. mid-span deflection, (mm)	(56.1, 55.0, -)
Max. end-span deflection, (mm)	(57.9, 60.5, -)
Bus assembly natural frequency, (Hz)	(2.63, 2.66, -)

Case 2 – Tennessee Valley Authority [19]

The results of fifteen short circuit tests were published. The bus initially had a butt weld in it. After the first seven tests, the bus had permanent deflection and bus was rolled over to maintain parallel position and decreased spacing. After an additional two tests, the bus was badly bent and had to be replaced. The bottom insulator of the insulator stack failed during the next test and then was replaced with a heavy-duty type insulator for one test. The last four tests had a standard type insulator. The results given are for the sixth and twelfth tests. Note that the bus specific weight is calculated based on the geometric data provided and a value of 2680 kg/m^3 for the density of the aluminum tubular conductor. The insulator spring constant is calculated based on the published cantilever force and the insulator deflection for test #6. When there is a difference in a parameter or test results between the tests, both values will given as (test 6 value, test 12 value).

Case 2 is represented by #4 and #5 on all plots.

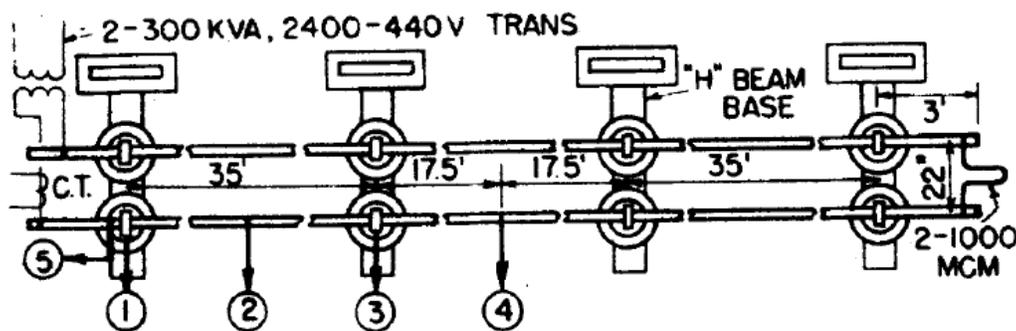**Figure 9-2**
Test Structure for Case 2 [19]

Table 9-6
Case 2 Electrical Parameters

Parameter Description	Value
Short Circuit Current, (kA RMS)	(33.3, 31.5)
Short Circuit Duration, (ms)	167
Ratio of system reactance to resistance, X/R	(6.20, 7.96)
Electrical frequency, Hz	60
Line-to-line fault	Y
Reclosure	N

Table 9-7
Case 2 Conductor Parameters

Parameter Description	Value
Bus conductor outer diameter, (mm)	101.6
Bus conductor wall thickness, (mm)	5.7
Bus conductor 2nd moment of area, (10^{-6} m^4)	1.993
Bus conductor section modulus, (10^{-5} m^3)	3.92
Bus conductor weight per unit length, (N/m)	45.4
Bus conductor modulus of elasticity (GPa)	69.0

Table 9-8
Case 2 Bus Assembly Parameters

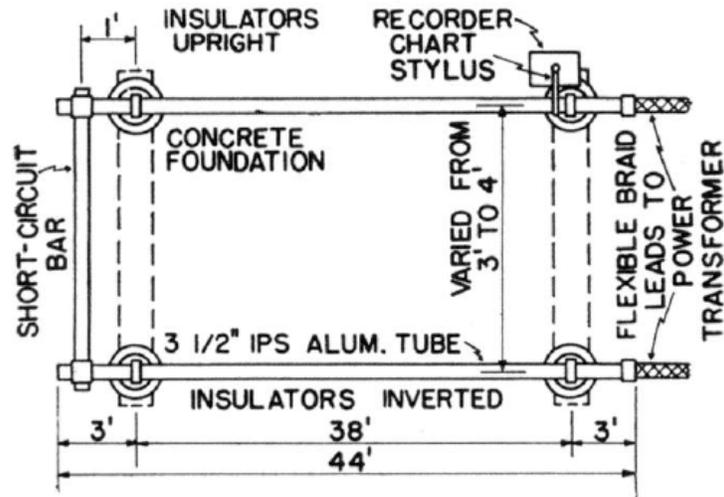| Parameter Description	Value
Phase center to phase center distance, (m)	1.22
Span length, (m)	11.58
Number of spans	1
Insulator spring constant, (N/mm)	142

Table 9-9
Case 2 Test Measurements

Measurement Description	Value
Max. inner insulator cantilever force, (N)	(3825 , 2847)
Max. outer insulator cantilever force, (N)	(3825, 2847)
Max. inner insulator deflection, (mm)	(26.99, 19.05)
Max. outer insulator deflection, (mm)	(26.99, 17.05)
Bus assembly natural frequency, (Hz)	(2.26, 1.43)

Case 3 – Ontario Hydro [7]

The result of one short circuit test was published. The testing employed a two span bus arrangement with 230 kV porcelain station post insulators on one phase (i.e. side) and 230 kV hollow-core composite insulators (HCI) on the other side. The results are given for the middle (i.e. inner) insulator for both insulator types. When there is a difference in a parameter or test results between the tests, both values are given as (value of bus w/ HCI, value of bus w/ porcelain insulator).

Case 3 is represented by #6 on all plots.

Figure 9-3
Test Structure for Case 3 [7]

Table 9-10
Case 3 Electrical Parameters

Parameter Description	Value
Short Circuit Current, (kA RMS)	34.7
Short Circuit Duration, (ms)	167
Ratio of system reactance to resistance, X/R	20.74
Electrical frequency, Hz	60
Line-to-line fault	Y
Reclosure	N

Table 9-11
Case 3 Conductor Parameters

Parameter Description	Value
Bus conductor outer diameter, (mm)	203.2
Bus conductor wall thickness, (mm)	7.1
Bus conductor 2nd moment of area, (10^{-6} m^4)	21.19
Bus conductor section modulus, (10^{-5} m^3)	20.85
Bus conductor weight per unit length, (N/m)	134.4
Bus conductor modulus of elasticity (GPa)	65.0

Table 9-12
Case 3 Bus Assembly Parameters

Parameter Description	Value
Phase center to phase center distance, (m)	1.0
Span length, (m)	13.63
Number of spans	2
Insulator spring constant, (N/mm)	(217, 517)

Table 9-13
Case 3 Test Measurements

Measurement Description	Value
Max. inner insulator cantilever force, (N)	(9400 , 3100)
Max. inner insulator deflection, (mm)	(43.4, 6)
Bus assembly natural frequency, (Hz)	(3.65, 4.70)

Case 4 – FGH Mannheim [20]

The result of one short circuit test was published where there was an initial short circuit followed by a reclosure. The testing employed a single-phase two span bus arrangement with 220 kV porcelain station post insulators. The results are given for the middle (i.e. inner) and outer insulator and steel supports for both the initial short circuit and the reclosure. When there is a difference in a parameter or test results between the tests, both values will given as (value for initial fault, value for reclosure).

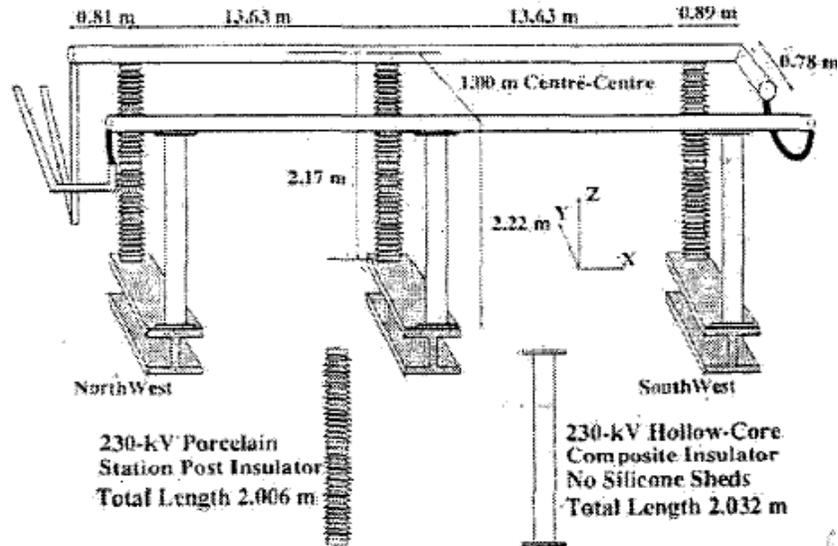Case 4 is represented by #7 on all plots.

Figure 9-4
Test Structure for Case 4 [20]

Table 9-14
Case 4 Electrical Parameters

Parameter Description	Value
Short Circuit Current, (kA RMS)	15.6
Short Circuit Duration, (ms)	(135, 305)
Ratio of system reactance to resistance, X/R	19.48
Electrical frequency, Hz	50
Line-to-line fault	Y
Reclosure	(N, Y)

Table 9-15
Case 4 Conductor Parameters

Parameter Description	Value
Bus conductor outer diameter, (mm)	121
Bus conductor wall thickness, (mm)	6.2
Bus conductor 2nd moment of area, (10^{-6} m^4)	3.700
Bus conductor section modulus, (10^{-5} m^3)	6.11
Bus conductor weight per unit length, (N/m)	59.2
Bus conductor modulus of elasticity (GPa)	70.0

Table 9-16
Case 4 Bus Assembly Parameters

Parameter Description	Value
Phase center to phase center distance, (m)	1.0
Span length, (m)	11.50
Number of spans	2
Insulator spring constant, (N/mm)	755

Table 9-17
Case 4 Test Measurements

Measurement Description	Value
Max. inner insulator cantilever force, (N)	(2425, 4635)
Max. outer insulator cantilever force, (N)	(773, 1501)
Max. inner steel support cantilever force, (N)	(2580, 4971)
Max. conductor stress, (MPa)	(37.7, 71.4)
Bus assembly natural frequency, (Hz)	3.42

Case 5 – Ontario Hydro [17]

The result of one short circuit test was published where there was an initial short circuit followed by a reclosure. The testing employed a three span bus arrangement with 500 kV porcelain station post insulators. The results are given for three middle (i.e. inner) insulators for both the initial fault (IF) and the reclosure (RC). When there is a difference in a parameter or test results between the SC tests, the values will given as (value for IF, value for RC) or (value for IF for pt. 151, value for IF for pt. 153, value for IF pt. 155, value for RC for pt. 151, value for RC for pt. 153, value for RC pt. 155).
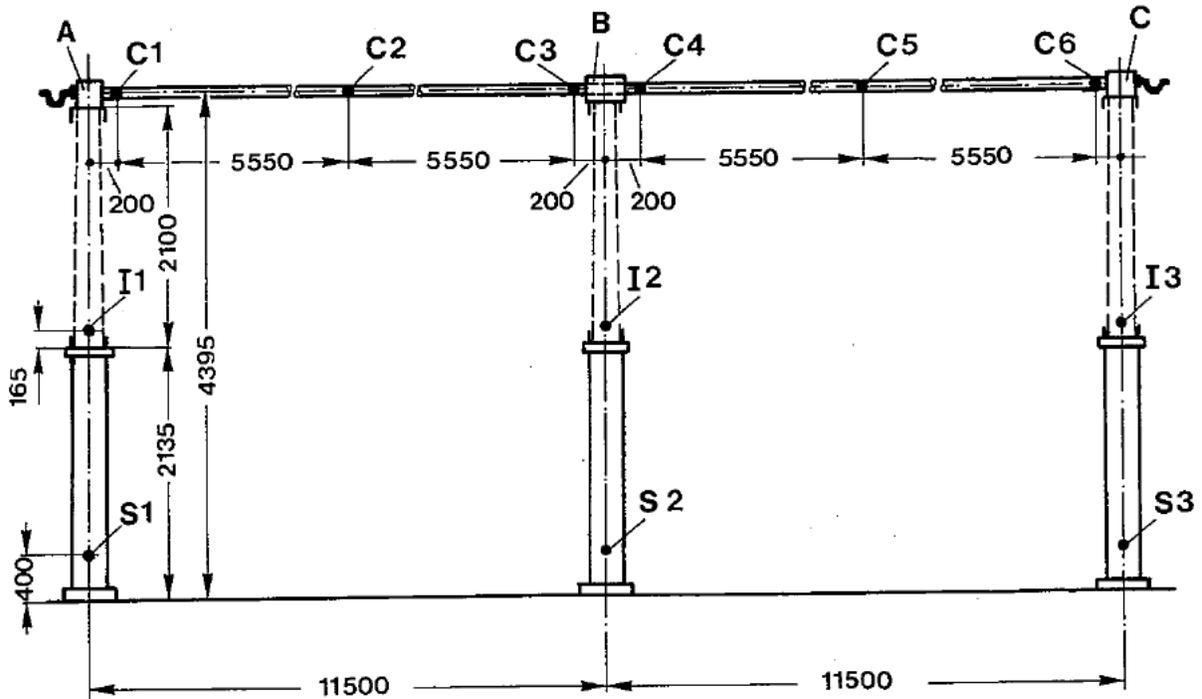
Case 5 is represented by #8 on all plots.

Figure 9-5
Test Structure for Case 5 [17]

Table 9-18
Case 5 Electrical Parameters

Parameter Description	Value
Short Circuit Current, (kA RMS)	(35.9, 35.7)
Short Circuit Duration, (ms)	(78, 136)
Ratio of system reactance to resistance, X/R	12.4
Electrical frequency, Hz	60
Line-to-line fault	Y
Reclosure	(N, Y)

Table 9-19
Case 5 Conductor Parameters

Parameter Description	Value
Bus conductor outer diameter, (mm)	200
Bus conductor wall thickness, (mm)	6.0
Bus conductor 2nd moment of area, (10^{-6} m^4)	17.22
Bus conductor section modulus, (10^{-5} m^3)	17.22
Bus conductor weight per unit length, (N/m)	97.1
Bus conductor modulus of elasticity (GPa)	65.0

Table 9-20
Case 5 Bus Assembly Parameters

Parameter Description	Value
Phase center to phase center distance, (m)	3.05
Span length, (m)	7.6
Number of spans	3
Insulator spring constant, (N/mm)	539

Table 9-21
Case 5 Test Measurements

Measurement Description	Value
Max. inner insulator cantilever force, (N)	(1023, 627, 783, 2122, 1530, 1713)
Max. inner insulator deflection, (mm)	(-, 9.1, 10.7,-, 20.8, 23.6)
Bus assembly natural frequency, (Hz)	(2.4, 2.7)

Case 6 – IREQ [21]

The result of one short circuit test was published where there was an initial short circuit followed by a reclosure. The testing employed a six span bus arrangement with 315 kV porcelain station post insulators. The results are given for the middle (i.e. inner) insulator and steel supports for both the initial fault (IF) and the reclosure (RC). The insulator strain was reported in μm/m without a conversion to force. The following formulas were used to relate the stain to the cantilever force:

$$\sigma = E\,\epsilon \tag{9.2}$$

$$FM = \frac{\sigma\,J}{y} \tag{9.3}$$

$$F = \frac{M}{l} = \frac{E\,\epsilon\,J}{y\,l} \tag{9.3}$$

where

> σ = the insulator bending stress, [kPa],
>
> E = the insulator modulus of elasticity, [GPa],
>
> ε = the insulator strain, [μm/m],
>
> M = the insulator bending moment, [kNm],
>
> J = the insulator 2nd moment of area, [m^4],
>
> y = the insulator displacement, [m],
>
> l = the insulator length, [m] and
>
> F = the insulator cantilever force, [kN],

When there is a difference in a parameter or test results between the SC tests, the values will given as (value for IF, value for RC).

Case 6 is represented by #9 on all plots.
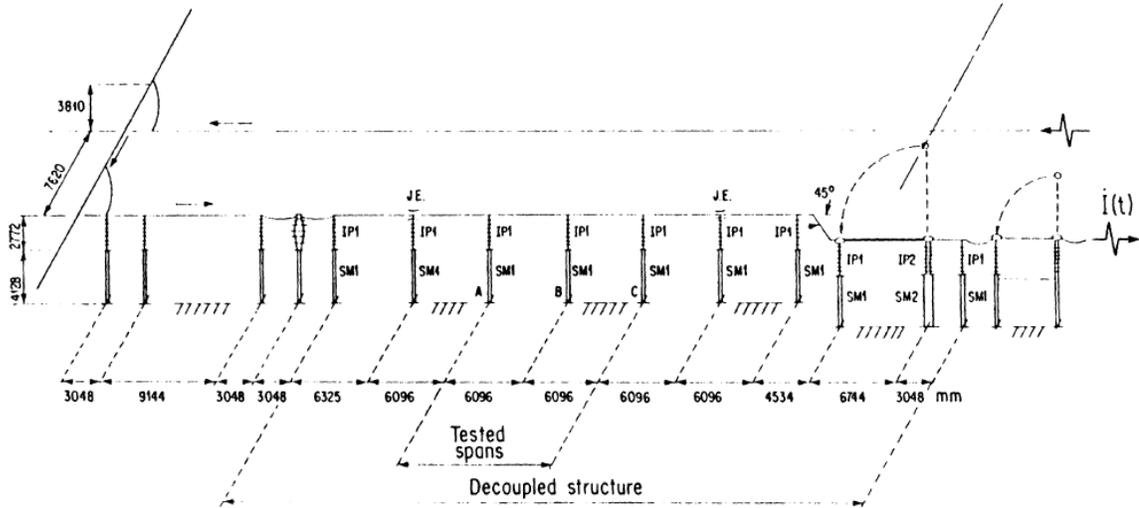
Figure 9-6
Test Structure for Case 6 [21]

Table 9-22
Case 6 Electrical Parameters

Parameter Description	Value
Short Circuit Current, (kA RMS)	(46.7)
Short Circuit Duration, (ms)	(212, 307)
Ratio of system reactance to resistance, X/R	1
Electrical frequency, Hz	50
Line-to-line fault	Y
Reclosure	(N, Y)

Table 9-23
Case 6 Conductor Parameters

Parameter Description	Value
Bus conductor outer diameter, (mm)	168.3
Bus conductor wall thickness, (mm)	7.1
Bus conductor 2nd moment of area, (10^{-6} m^4)	11.7
Bus conductor section modulus, (10^{-5} m^3)	13.9
Bus conductor weight per unit length, (N/m)	94.5
Bus conductor modulus of elasticity (GPa)	65.0

Table 9-24
Case 6 Bus Assembly Parameters

Parameter Description	Value
Phase center to phase center distance, (m)	1.62
Span length, (m)	6.1
Number of spans	6
Insulator spring constant, (N/mm)	119

Table 9-25
Case 6 Test Measurements

Measurement Description	Value
Max. inner insulator cantilever force, (N)	(2567, 2904)
Max. inner insulator insulator deflection, (mm)	(21.5, 34)
Max. inner steel support deflection, (mm)	(8, 13.5)
Bus assembly natural frequency, (Hz)	2.4

Case 7 – FGH Mannheim [22]

The result of one short circuit test was published. The testing employed a three span bus arrangement with very stiff station post insulators with a natural frequency close to the power system frequency (i.e. 58.9 Hz vs. 50 Hz). The results are given for the middle (i.e. inner) insulator.

Case 7 is represented by #A on all plots.

Figure 9-7
Test Structure for Case 7 [22]

Table 9-26
Case 7 Electrical Parameters

Parameter Description	Value
Short Circuit Current, (kA RMS)	7.5
Short Circuit Duration, (ms)	300
Ratio of system reactance to resistance, X/R	29.85
Electrical frequency, Hz	50
Line-to-line fault	Y
Reclosure	N

Table 9-27
Case 7 Conductor Parameters

Parameter Description	Value
Bus conductor outer diameter, (mm)	30
Bus conductor wall thickness, (mm)	5
Bus conductor 2nd moment of area, (10^{-6} m^4)	0.032
Bus conductor section modulus, (10^{-5} m^3)	0.213
Bus conductor weight per unit length, (N/m)	10.4
Bus conductor modulus of elasticity (GPa)	70.0

Table 9-28
Case 7 Bus Assembly Parameters

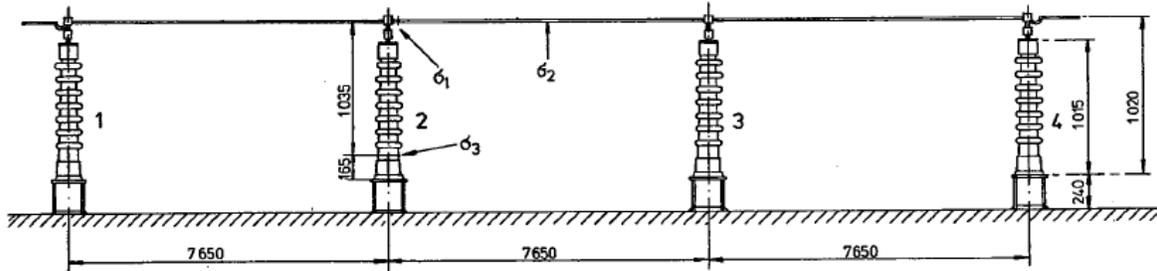| Parameter Description	Value
Phase center to phase center distance, (m)	1.0
Span length, (m)	7.65
Number of spans	3
Insulator spring constant, (N/mm)	1960

Table 9-29
Case 7 Test Measurements

Measurement Description	Value
Max. inner insulator cantilever force, (N)	413
Max. conductor stress, (MPa)	64.5
Bus assembly natural frequency, (Hz)	58.9

Case 8 –ENEL [22]

The result of one short circuit test was published. The testing employed a three span bus arrangement with a very flexible bus assembly. The results are given for the middle (i.e. inner) insulator.

Case 8 is represented by #B on all plots.

Figure 9-8
Test Structure for Case 8 [22]

Table 9-30
Case 8 Electrical Parameters

Parameter Description	Value
Short Circuit Current, (kA RMS)	45.0
Short Circuit Duration, (ms)	1030
Ratio of system reactance to resistance, X/R	12.57
Electrical frequency, Hz	50
Line-to-line fault	Y
Reclosure	N

Table 9-31
Case 8 Conductor Parameters

Parameter Description	Value
Bus conductor outer diameter, (mm)	220
Bus conductor wall thickness, (mm)	6.5
Bus conductor 2nd moment of area, (10^{-6} m^4)	24.86
Bus conductor section modulus, (10^{-5} m^3)	22.6
Bus conductor weight per unit length, (N/m)	115.7
Bus conductor modulus of elasticity (GPa)	70.5

Table 9-32
Case 8 Bus Assembly Parameters

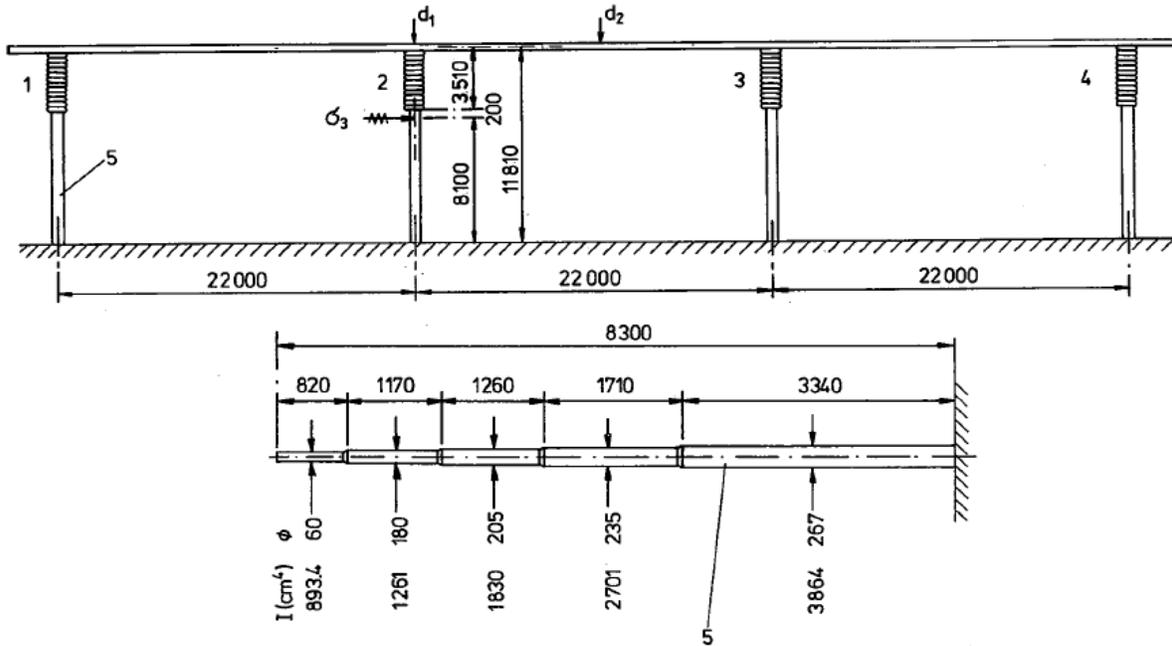| Parameter Description	Value
Phase center to phase center distance, (m)	5.5
Span length, (m)	22.0
Number of spans	3
Insulator spring constant, (N/mm)	405

Table 9-33
Case 8 Test Measurements

Measurement Description	Value
Max. inner insulator cantilever force, (N)	1898
Max. inner insulator deflection, (mm)	415.0
Max. mid-span deflection, (mm)	405.0
Bus assembly natural frequency, (Hz)	0.96

Case 9 –EdF [22]

The result of one short circuit test was published. The testing employed a three span bus arrangement. The results are given for the middle (i.e. inner) insulator.

Case 9 is represented by #C on all plots.

Figure 9-9
Test Structure for Case 9 [22]

Table 9-34
Case 9 Electrical Parameters

Parameter Description	Value
Short Circuit Current, (kA RMS)	64.3
Short Circuit Duration, (ms)	500
Ratio of system reactance to resistance, X/R	14.14
Electrical frequency, Hz	50
Line-to-line fault	Y
Reclosure	N

Table 9-35
Case 9 Conductor Parameters

Parameter Description	Value
Bus conductor outer diameter, (mm)	200
Bus conductor wall thickness, (mm)	8.0
Bus conductor 2nd moment of area, (10^{-6} m⁴)	22.27
Bus conductor section modulus, (10^{-5} m³)	22.27
Bus conductor weight per unit length, (N/m)	127.5
Bus conductor modulus of elasticity (GPa)	65.0

Table 9-36
Case 9 Bus Assembly Parameters

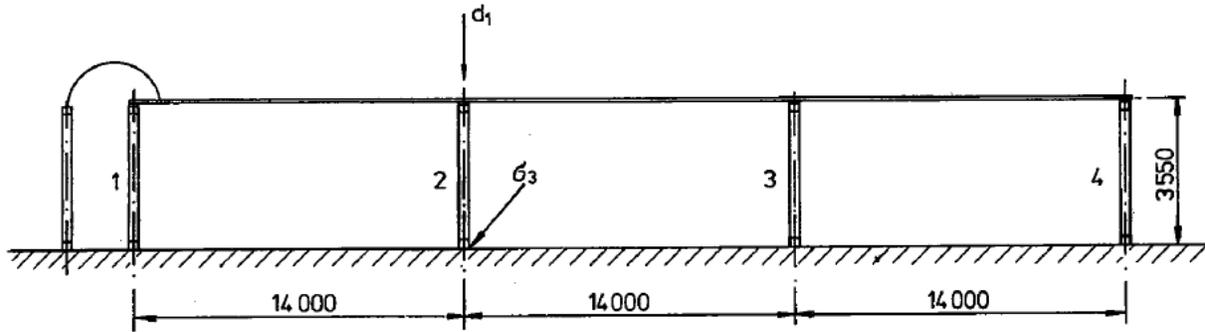| Parameter Description	Value
Phase center to phase center distance, (m)	7.5
Span length, (m)	14.0
Number of spans	3
Insulator spring constant, (N/mm)	104

Table 9-37
Case 9 Test Measurements

Measurement Description	Value
Max. inner insulator cantilever force, (N)	5521
Max. inner insulator deflection, (mm)	53

10
COMPARATIVE STUDY OF ADVANCED SC FORCE PREDICTION METHODS

Hosemann and Tsanakas provide insight into the accuracy of Attri and Edgar's method in their paper comparing predictions of dynamic short circuit stress in a high-voltage test structure with test measurements [20]. This seminal comparative study was carried out by Working Group 2 of CIGRE-Study Committee No. 23. The test structure, shown in Figure 9-4, is cited in Annex F of IEEE Std. 605 [3] as the CIGRE Structure D.

The authors gathered predictions from 10 different computer programs/advanced calculation techniques of the maximum and time-varying values of bending moment on the insulators, supports, and conductors of the bus structure. These model predictions were then compared with measurements of the same quantities on an actual bus structure of the same type. Dynamic response models from the following 10 firms, agencies or research groups were considered:

1. ASEA, Sweden
2. ENEL, Italy
3. Imatran Voima, Finland
4. KEMA, The Netherlands
5. Ontario Hydro, Canada
6. Siemens, Germany
7. SSPB, Sweden, and
8. Erlangen University, Germany (three codes provided: Transfer method, Analytical Method, and VDE 0103).

Model complexity varied widely. Three of the models did not require a computer to evaluate (i.e., Ontario Hydro, SSPB, and VDE 0103). The more complex approaches included step-by-step integration of the differential equations describing the mechanical system, superposition of modes of oscillations resulting from the various natural frequencies of the mechanical system, and finite element analysis of a system of ideal elastic elements with a uniform distribution of masses.

Hosemann and Tsanakas describe one of the 10 methods, i.e., the Ontario Hydro model, as a methodology that derives bus dynamic stress from static stress through the application of frequency-dependent factors derived by the methodology presented in Attri and Edgar's paper [4].

Figures 8 and 9 (reproduced as Figure 10-1 and Figure 10-2) present some of the results of the measurement program described in [20]. For the maximum bending moment of the Structure D steel pillars and insulators, Figure 10-1 compares the absolute percent deviation of predicted values from measured values at six different measurement points, for each of the ten methods that were evaluated. Figure 10-2 provides a similar comparison for the maximum bending stress in the conductors. In order to highlight the performance of the Ontario Hydro model (i.e., Attri and Edgar methodology), its data bars are marked with black dots.

The largest deviations among the data were about 21% for the maximum bending moment in the support structure and in the maximum bending stress in the conductor. For the Ontario Hydro model, the largest, smallest, and average deviations for the maximum bending moment on insulators were 15, 7.5, and 11.8 percent respectively. The largest, smallest, and average deviations for the maximum conductor bending stress were 12, 2, and 6.8 percent respectively. Hosemann and Tsanakas noted on p. 158 of [18] from these results that "the maximum values obtained from the three simple methods not using a computer program (Ontario Hydro, SSPB and VDE0103) show deviations from the measured values similar to those obtained by means of extensive computation programs". They reinforce this observation by closing their paper on page 160 with this comment: "A noteworthy fact is that the three simple calculation methods provided similarly accurate results as the extensive computer programs."
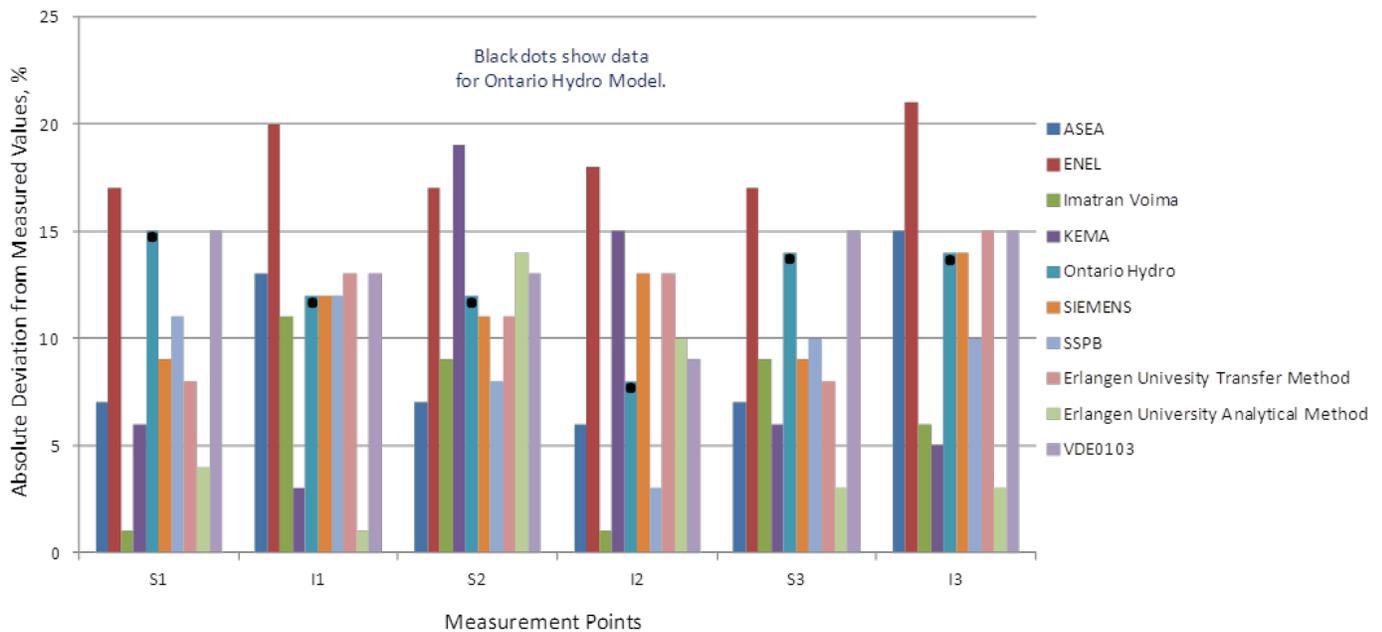
Figure 10-1
Comparison of Ten Advanced SC Force Models for Maximum bending moment in steel pillars and insulators – No reclosure
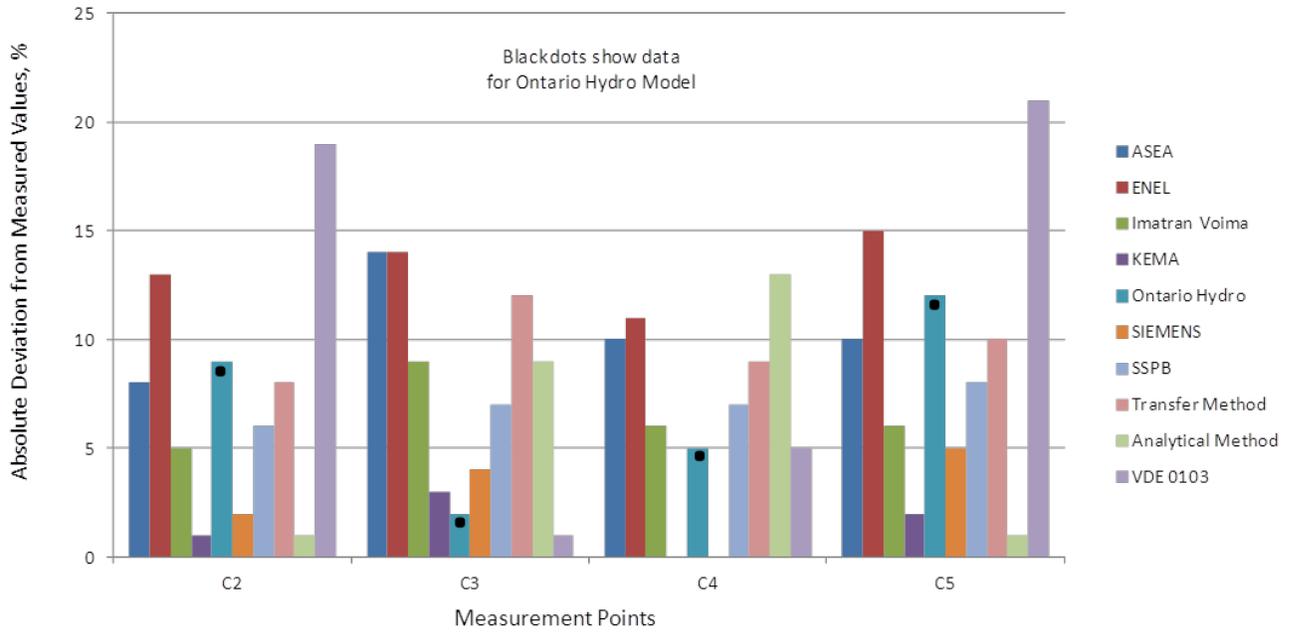
Figure 10-2
Comparison of Ten Advanced SC Force Models for Maximum bending stress in conductor – No reclosure

11
COMPUTER CODE FOR ATTRI-EDGAR METHOD

Attri-Edgar Method User's Guide

The MATLAB for the Attri-Edgar Method is written with the documentation built in. In order to understand how to use it, consult the function's help by typing help and the name of the function such as 'help AE_SC_Force'. The main SC force calculation function uses three other functions:

1. Edgar_Nat_Freq

2. Calc_N_Factor

3. Support_Factors

Attri-Edgar Short Circuit Force Calculation

```
function F_SC = AE_SC_Force(varargin)
%
% AE_SC_Force - Calculates the short circuit force on the conductor and
% insulators using the Attri-Edgar method (i.e. based on NEMA SC force
% calc) and Attri-Edgar dynamic factor, N, given the following inputs:
%
% 1. the symmetrical RMS current, I_SC [A]
% 2. power frequency, fp [Hz]
% 3. measured mechanical frequency of the bus, f [Hz]
% 4. ratio of system reactance to system resistance, XbyR
% 5. the distance between bus bars, S [in]
% 6. the span length, L [m]
% 7. the number of spans, Nsp
% 8. the outer insulator support and bus mass, M_a [kg]
% 9. the inner insulator support and bus mass, M_b [kg]
% 10. the insulator support spring constant, Ki [N/mm]
% 11. the bus conductor modulus of elasticity/Young's Modulus, E_bus [GPa]
% 12. the bus conductor 2nd moment of area, I_bus [m4]
% 13. the bus conductor section modulus, S_bus [m3]
% 14. a flag indicating whether or not the fault is line-to-line or not
% 15. a flag indicating whether or not to use the calc. bus freq.
% 16. a flag indicating whether or not to include the effects of automatic
%     reclosing
% 17. the busbar support arrangement, SA
%
% SA = 0 => single span, simple supports
% SA = 1 => single span, fixed support, simple support
% SA = 2 => single span, fixed supports
% SA = 3 => two spans, simple supports
% SA = 4 => three or more spans, simple supports
%
% Returns the value of the SC insulator support forces for the outer
% conductor, [N] and conductor bending stress, [MPa]
%
% Constants
N2LBF = 1/4.448;
```

```matlab
M2IN = 12*3.2808;
FT2IN = 12;
M2FT = 3.2808;
G = 0.866;      % Factor for three-phase faults
C_fs = 3.46;    % Conversion factor for English units for bending stress
                % from IEEE 605-1998
%
% Inputs
I_SC = varargin{1};
fp = varargin{2};
f = varargin{3};
XbyR = varargin{4};
S = varargin{5}*M2IN;
L = varargin{6}*M2FT; L_in = L*FT2IN;
Nsp = varargin{7};
M_a = varargin{8};
M_b = varargin{9};
Ki = varargin{10};
E_bus = varargin{11};
I_bus = varargin{12};
S_bus = varargin{13}; S_bus = S_bus*M2IN^3;
LL_flag = varargin{14};
f_calc_flag = varargin{15};
RC_flag = varargin{16};
SA = varargin{17};
%
% Natural frequency
if (f_calc_flag)
    f = Edgar_Nat_Freq(E_bus,I_bus,L,Nsp,M_a,M_b,Ki);
end
%
% Dynamic factor
N = Calc_N_Factor(fp,f,XbyR,LL_flag);
if (RC_flag)
    Nr = 2;
else
    Nr = 1;
end
%
% Static SC force
if (LL_flag)
    Fd = Nr*N(1)*43.2*I_SC^2/(S*1E7);
else
    Fd = Nr*N(1)*G*43.2*I_SC^2/(S*1E7);
end
%
% Conductor bending stress
if (SA < 2 || SA == 3)
    Sig = (L_in/C_fs)^2*Fd/(8*S_bus);
elseif (SA == 2)
    Sig = (L_in/C_fs)^2*Fd/(12*S_bus);
else
    if (Nsp == 3)
        Sig = (L_in/C_fs)^2*Fd/(10*S_bus);
    elseif (Nsp == 4)
        Sig = (L_in/C_fs)^2*Fd/(28*S_bus);
    else % best assumption for this case
```

```
        Sig = (L_in/C_fs)^2*Fd/(28*S_bus);
    end
end
Sigma = Sig*(M2IN^2)/N2LBF/1E6;
%
% cantilever force
abg = Support_Factors(SA);
Fs_a = abg(1)*L*Fd;
Fs_b = abg(2)*L*Fd;
%
F_SC = [Fs_a/N2LBF Fs_b/N2LBF Sigma];
%
end
```

Attri-Edgar Bus Assembly Natural Frequency Calculation

```
function f = Edgar_Nat_Freq(varargin)
%
% f = Edgar_Nat_Freq(E,J,l,m)
% Outputs the Edgar Method bus natural frequency, f given
%
% This approach assumes equidistant supports.
%
% 1. busbar's Young's modulus/modulus of elasticity, E [GPa]
% 2. busbar's moment of inertia, J [m4]
% 3. busbar's span length, l [m]
% 4. the number of spans, Nsp
% 5. outer insulator support & bus mass, M_a [kg]
% 6. inner insulator support & bus mass, M_b [kg]
% 7. insulator support spring constant, Ki [N/mm]
%
% Returns the bus natural frequency, f [Hz]
%
g = 9.807;
GPa2Pa = 10^9;
mm2m = 1000;
%
E = varargin{1}; E = E*GPa2Pa;
J = varargin{2};
l = varargin{3};
Nsp = varargin{4};
M_a = varargin{5};
M_b = varargin{6};
Ki = varargin{7}; Ki = Ki*mm2m;
%
L = l*Nsp;
x_off = 1;
if (Nsp == 1)
    M_sum = M_a+M_b;
    K_sum = 2*Ki;
    ksi = [x_off x_off+l];
elseif (Nsp == 2);
    M_sum = 2*M_a+M_b;
    K_sum = 3*Ki;
    ksi = [x_off x_off+l x_off+2*l];
elseif (Nsp == 3)
    M_sum = 2*M_a+2*M_b;
```

```matlab
    K_sum = 4*Ki;
    ksi = [x_off x_off+l x_off+2*l x_off+3*l];
elseif (Nsp == 4)
    M_sum = 2*M_a+3*M_b;
    K_sum = 5*Ki;
    ksi = [x_off x_off+l x_off+2*l x_off+3*l x_off+4*l];
elseif (Nsp == 5)
    M_sum = 2*M_a+4*M_b;
    K_sum = 6*Ki;
    ksi = [x_off x_off+l x_off+2*l x_off+3*l x_off+4*l x_off+5*l];
elseif (Nsp == 6)
    M_sum = 2*M_a+5*M_b;
    K_sum = 7*Ki;
    ksi = [x_off x_off+l x_off+2*l x_off+3*l x_off+4*l x_off+5*l x_off+6*l];
end
%
Ksi_sum = 0;
for i = 1:length(ksi)
    Ksi_sum = Ksi_sum + ksi(i)^2*(L-ksi(i))^2;
end
f = sqrt( (3*E*J*L/Ksi_sum/M_sum)+K_sum/M_sum )/(2*pi);
%
end
```

Attri-Edgar N Factor Calculation

```matlab
function N = Calc_N_Factor(varargin)
%
% N = Calc_N_Factor(fp,f,XbyR,LL_flag)
% Calculates the N factor given the following:
%
% 1. power frequency, fp, in [Hz]
% 2. mechanical frequency of the bus, f, in [Hz]
% 3. ratio of system reactance to system resistance, XbyR
% 4. a flag indicating whether or not the fault was line-to-line or not
%
% Returns the value of the Attri-Edgar N factor
%
A = load('N_FACT_RAW.mat');
%
fp = varargin{1};
f = varargin{2};
XbyR = varargin{3};
LL_flag = varargin{4};
%
f_ratio = (fp*2*pi/XbyR)*(1/(f*2*pi));
if (LL_flag)
    if (f_ratio > 2.5)
        N(1) = 0.251;
    else
        ind = A.N_FACT_RAW(:,1)>0;
        w_p_by_w = A.N_FACT_RAW(ind,1);
        N_LL = A.N_FACT_RAW(ind,2);
        N(1) = interp1(w_p_by_w,N_LL,f_ratio);
    end
    N(2) = 0;
    N(3) = 0;
```

```matlab
    else
        if (f_ratio > 2.5)
            N(1) = 0.2;
            N(2) = 0.053;
            N(3) = 0.2;
        else
            ind_A = A.N_FACT_RAW(:,4)>0;
            ind_B = A.N_FACT_RAW(:,6)>0;
            w_p_by_w_A = A.N_FACT_RAW(ind_A,3);
            w_p_by_w_B = A.N_FACT_RAW(ind_B,5);
            N_3PH_ctr_A = A.N_FACT_RAW(ind_A,6);
            N_3PH_o_B = A.N_FACT_RAW(ind_B,6);
            N(1) = interp1(w_p_by_w_B,N_3PH_o_B,f_ratio);
            N(2) = interp1(w_p_by_w_A,N_3PH_ctr_A,f_ratio);
            N(3) = 0.2;
        end
end
end
```

Calculation of Support Factors

```matlab
function abg = Support_Factors(varargin)
%
% abg = Support_Factors(SA)
% Outputs the busbar support arrangement factors alpha_a, alpha_b, beta,
% gamma given
%
% 1. the busbar support arrangement, SA
%
% SA = 0 => single span, simple supports
% SA = 1 => single span, fixed support, simple support
% SA = 2 => single span, fixed supports
% SA = 3 => two spans, simple supports
% SA = 4 => three or more spans, simple supports
%
% Returns the value of the support arrangement factors
%
SA = varargin{1};
%
if (SA==0)
    alpha_a = 0.5;
    alpha_b = 0.5;
    beta = 1;
    gamma = 1.57;
elseif (SA==1)
    alpha_a = 0.625;
    alpha_b = 0.375;
    beta = 0.73;
    gamma = 2.45;
elseif (SA==2)
    alpha_a = 0.5;
    alpha_b = 0.5;
    beta = 0.5;
    gamma = 3.56;
elseif (SA==3)
```

```matlab
    alpha_a = 0.375;
    alpha_b = 1.25;
    beta = 0.73;
    gamma = 2.45;
else
    alpha_a = 0.4;
    alpha_b = 1.1;
    beta = 0.73;
    gamma = 3.56;
end
abg = [alpha_a alpha_b beta gamma];
%
end
```

Export Control Restrictions

Access to and use of EPRI Intellectual Property is granted with the specific understanding and requirement that responsibility for ensuring full compliance with all applicable U.S. and foreign export laws and regulations is being undertaken by you and your company. This includes an obligation to ensure that any individual receiving access hereunder who is not a U.S. citizen or permanent U.S. resident is permitted access under applicable U.S. and foreign export laws and regulations. In the event you are uncertain whether you or your company may lawfully obtain access to this EPRI Intellectual Property, you acknowledge that it is your obligation to consult with your company's legal counsel to determine whether this access is lawful. Although EPRI may make available on a case-by-case basis an informal assessment of the applicable U.S. export classification for specific EPRI Intellectual Property, you and your company acknowledge that this assessment is solely for informational purposes and not for reliance purposes. You and your company acknowledge that it is still the obligation of you and your company to make your own assessment of the applicable U.S. export classification and ensure compliance accordingly. You and your company understand and acknowledge your obligations to make a prompt report to EPRI and the appropriate authorities regarding any access to or use of EPRI Intellectual Property hereunder that may be in violation of applicable U.S. or foreign export laws or regulations.

The Electric Power Research Institute, Inc. (EPRI, www.epri.com) conducts research and development relating to the generation, delivery and use of electricity for the benefit of the public. An independent, nonprofit organization, EPRI brings together its scientists and engineers as well as experts from academia and industry to help address challenges in electricity, including reliability, efficiency, health, safety and the environment. EPRI also provides technology, policy and economic analyses to drive long-range research and development planning, and supports research in emerging technologies. EPRI's members represent approximately 90 percent of the electricity generated and delivered in the United States, and international participation extends to more than 30 countries. EPRI's principal offices and laboratories are located in Palo Alto, Calif.; Charlotte, N.C.; Knoxville, Tenn.; and Lenox, Mass.

Together…Shaping the Future of Electricity

1024226